BOREAS An international journal of Quaternary research

Hydroclimatic development from the Early Holocene to anthropogenic times: a comparative study of diatom oxygen isotope records and multiproxy data from Lake Khamra, eastern Siberia

AMELIE STIEG, BORIS K. BISKABORN, ULRIKE HERZSCHUH, JENS STRAUSS, SVETLANA S. KOSTROVA, LUIDMILA A. PESTRYAKOVA AND HANNO MEYER

BOREAS

Stieg, A., Biskaborn, B. K., Herzschuh, U., Strauss, J., Kostrova, S. S., Pestryakova, L. A. & Meyer, H.: Hydroclimatic development from the Early Holocene to anthropogenic times: a comparative study of diatom oxygen isotope records and multiproxy data from Lake Khamra, eastern Siberia. *Boreas*. https://doi.org/10.1111/bor.70022. ISSN 0300-9483.

Northern Eurasia underwent major hydroclimatic changes since the beginning of the Holocene interglacial. A rapid warming period reaching the Holocene Thermal Maximum (HTM), followed by a general cooling trend until recent times, was observed in Eurasian lacustrine diatom oxygen isotope ($\delta^{18}O_{diatom}$) records. In this study, we present a new Holocene $\delta^{18}O_{diatom}$ record from Lake Khamra (59.99°N, 112.98°E, Siberia). Our record aligns with Holocene $\delta^{18}O_{diatom}$ records across the Northern Hemisphere, showing a general millennial-scale cooling trend following an initial maximum at 11.2 cal. ka BP and a second maximum at 6.7 cal. ka BP. These maxima correspond to the summer insolation maximum and elevated Northern Hemisphere air temperatures, as well as increased bioproductivity. Variability on centennial scales is likely driven by precipitation changes, which coincide with higher sedimentation rates and overlay the general decreasing trend throughout the Holocene. In addition, we compared two multiproxy datasets with decadal resolution from Lake Khamra, including $\delta^{18}O_{diatom}$ data and biogeochemical proxies such as total organic carbon (TOC), total nitrogen (TN), stable carbon ($\delta^{13}C$) and nitrogen ($\delta^{15}N$) isotopes, and total mercury (THg). The datasets cover a ~210-year period (*c*. 6.140–6.350 cal. ka BP) at the end of the HTM and a recently published ~220-year record (*c*. 1790–2015 CE) that embraces the anthropogenic times. The comparison of these two warm phases reveals distinct differences in both the absolute values and the variability of the records. Regarding the $\delta^{18}O_{diatom}$ data, the recent period shows a nearly threefold increase in range and double the standard deviation, suggesting greater hydroclimatic variability compared to the end of the HTM. Notably, THg levels indicate a sharp increase in recent decades, while $\delta^{13}C$ declined, contrasting with the observations at the end of the HTM. We attribute these observations partially to far-reaching anthropogenic effects on remote lake systems.

Amelie Stieg (amelie.stieg@awi.de), Alfred Wegener Institute, Helmholtz Centre for Polar and Marine Research, Telegrafenberg A45, Potsdam 14473, Germany and Institute of Environmental Science and Geography, University of Potsdam, Potsdam 14476, Germany; Boris K. Biskaborn, Jens Strauss and Hanno Meyer, Alfred Wegener Institute, Helmholtz Centre for Polar and Marine Research, Telegrafenberg A45, Potsdam 14473, Germany; Ulrike Herzschuh, Alfred Wegener Institute, Helmholtz Centre for Polar and Marine Research, Telegrafenberg A45, Potsdam 14473, Germany, Institute of Environmental Science and Geography, University of Potsdam, Potsdam 14476, Germany and Institute of Biochemistry and Biology, University of Potsdam, Potsdam 14476, Germany; Svetlana S. Kostrova, Weizman Institute of Science, Department of Earth and Planetary Sciences, Rehovot 7610001, Israel; Luidmila A. Pestryakova, Institute of Natural Sciences, North-Eastern Federal University, Belinsky Str. 58, Yakutsk 677000, Russia; *received 2nd October 2024, accepted 29th May 2025.*

Northern latitudes experienced substantial hydroclimatic changes since the start of the Holocene (Kaufman *et al*. 2020; Herzschuh *et al*. 2023), which is generally dated to 11.65 ka BP (thousand years before present, referring to the year 1950 CE, Common Era), as derived from the Greenland NGRIP2 ice core (Walker *et al*. 2009). In the last decades, the northern latitudes have undergone rapid warming, at rates almost four times higher than the rest of the globe (Rantanen *et al*. 2022). This recent warming has been accompanied by permafrost thawing (Biskaborn *et al*. 2019; Czerniawska & Chlachula 2020), tree line migration (MacDonald *et al*. 2008), increasing wildfires (Kirillina *et al*. 2020; Scholten *et al*. 2022) and it affects lake systems (Woolway *et al*. 2020; Huang *et al*. 2022), as also identified in Siberia (Roberts *et al*. 2018; Biskaborn *et al*. 2021b; Stieg *et al*. 2024b), raising concerns about natural water resources.

Conditions during the Early Holocene were quite different and are described as colder than today, with moist summer conditions (Nazarova *et al*. 2013) and prolonged seasonal lake ice cover (Biskaborn *et al*. 2016) in eastern Siberia. At Lake Khamra (59.99°N, 112.98°E), in the Republic of Sakha (Yakutia) in eastern Siberia (Fig. 1A), long-term shifts in aquatic and terrestrial ecosystems over the Holocene have been observed (Baisheva *et al*. 2024). At this site, the onset of the Holocene is identified at 11.2 cal. ka BP (calibrated thousand years BP), with the Early Holocene (11.2–8.2 cal. ka BP) characterised by warmer and wetter conditions, increased bioproductivity and denser vegetation cover compared to the preceding Pleistocene (Baisheva *et al*. 2024). Following the Early Holocene, air temperatures rapidly increased towards the Mid-Holocene, reaching a Holocene Thermal Maximum (HTM) that varied spatially and temporally between approximately

DOI 10.1111/bor.70022

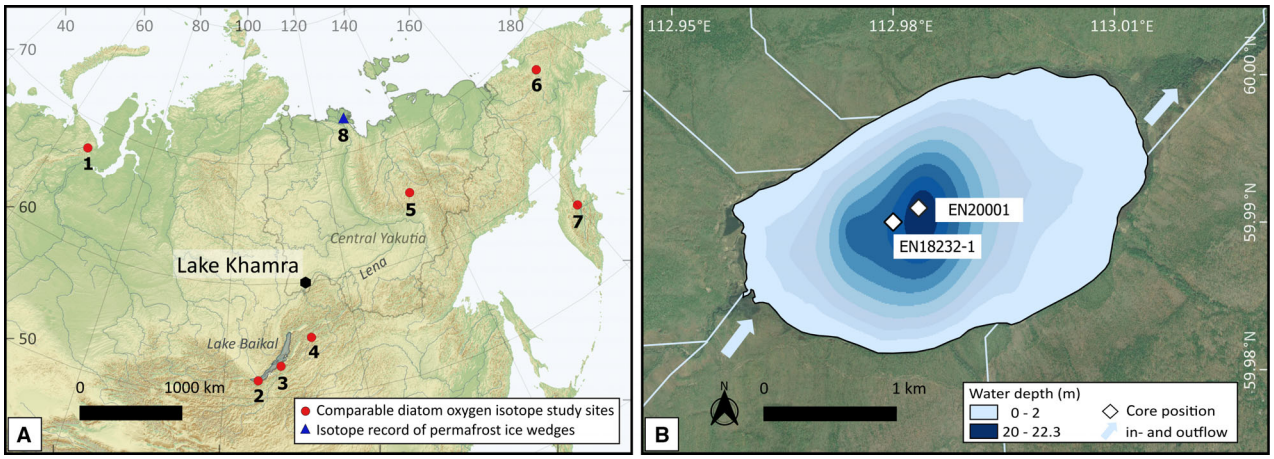

Fig. 1. A. Location of Lake Khamra (59.99°N, 112.98°E) in SW Yakutia, Siberia, with other Holocene $\delta^{18}O_{diatom}$ study sites mentioned in the text: 1 = Lake Bolshoye Shchuchye in the Polar Urals (Meyer *et al.* 2022); 2 = Lake Baikal (Mackay *et al.* 2011); 3 = Lake Kotokel (Kostrova *et al.* 2013b); 4 = Lake Baunt (Harding *et al.* 2020); 5 = Lake Emanda (Kostrova *et al.* 2021); 6 = Lake El'gygytgyn (Swann *et al.* 2010; Chapligin *et al.* 2012b); 7 = Two-Yurts Lake in Kamchatka (Meyer *et al.* 2015a); and 8 = $\delta^{18}O$ record of permafrost ice wedges in the Lena River delta, a winter temperature proxy (Meyer *et al.* 2015b). B. Bathymetry of Lake Khamra, with main inflow in the SW and outflow in the NE and drilling position of the sediment cores EN20001 and EN18232-1 in the central part of the lake. Service layer credits: Esri, Maxar, Earthstar Geographics and the GIS User Community.

8.9 and 4.5 cal. ka BP in north-eastern Siberia (Biskaborn *et al.* 2016). At Lake Khamra, the highest peak of bioproductivity is observed between 8.2 and 6 cal. ka BP during the Mid-Holocene, coinciding with a decrease in lake level and the presence of diatom taxa indicative of warm conditions (Baisheva *et al.* 2024). In the Late Holocene, after approximately 4.5 cal. ka BP, a cooling trend is observed (Biskaborn *et al.* 2016; Baisheva *et al.* 2024), accompanied by the establishment of a mixed evergreen-summergreen forest, similar to present-day conditions (Baisheva *et al.* 2024).

Subetto *et al.* (2017) provided an overview of palaeolimnological studies across northern Eurasia. In eastern Siberia, numerous studies have utilised a range of proxies to reconstruct Holocene and pre-Holocene environmental conditions. These proxies include pollen or chironomid analysis (Müller *et al.* 2010; Nazarova *et al.* 2013; Tarasov *et al.* 2013; Andreev *et al.* 2022), biogeochemical indicators (Baumer *et al.* 2020; Hughes-Allen *et al.* 2021), macroscopic charcoal records for palaeo-fire reconstruction (Glückler *et al.* 2021, 2022), multiproxy approaches (Diekmann *et al.* 2016; Biskaborn *et al.* 2021c) or sedimentary ancient DNA (Courtin *et al.* 2021; Baisheva *et al.* 2023). In addition, diatoms, unicellular microalgae with a cell wall made of biogenic silica ($SiO_2 \times nH_2O$), are valuable indicators for palaeoclimate conditions in Siberia (Biskaborn *et al.* 2012, 2013; Pestryakova *et al.* 2012, 2018).

Oxygen isotopes of diatoms ($\delta^{18}O_{diatom}$) analysed in lake sediment records are a powerful proxy for reconstructing past hydroclimate (Leng & Barker 2006). A global compilation of lacustrine $\delta^{18}O_{diatom}$ records indicates that most studies are focused on the Holocene, revealing a common long-term climate trend following decreasing summer insolation and air temperatures in the Northern Hemisphere (Meister *et al.* 2024). Particularly in Asia, more than 20 diatom oxygen isotope records have been published (Meister *et al.* 2024). In Siberia, several studies of $\delta^{18}O_{diatom}$ covering the Holocene are available, progressing from western Eurasia (Kostrova *et al.* 2019; Meyer *et al.* 2022) to the east (Kostrova *et al.* 2021) and the Russian Far East (Swann *et al.* 2010; Chapligin *et al.* 2012b) towards Central Kamchatka (Meyer *et al.* 2015a). Southern Siberia, particularly the Lake Baikal region, has been extensively studied (Kalmychkov *et al.* 2007; Mackay *et al.* 2011; Kostrova *et al.* 2013a, 2016; Swann *et al.* 2018; Harding *et al.* 2020). However, the coverage of $\delta^{18}O_{diatom}$ records in continental eastern Siberia, particularly between Central Yakutia and Lake Baikal, remains limited, highlighting the need for additional data to improve reconstructions of Holocene hydroclimatic conditions (Fig. 1A).

A limited number of diatom records (isotopes and assemblages) address particular modern climate change and its impact on lake ecosystems, for example, in eastern Siberia or at Lake Baikal (e.g. Roberts *et al.* 2018; Biskaborn *et al.* 2021b; Stieg *et al.* 2024a, b). On short-term scales, the sub-decadal $\delta^{18}O_{diatom}$ record from Lake Khamra reveals winter precipitation as a key driver over the last *c.* 220 years (Stieg *et al.* 2024b), contrasting with the long-term Holocene influence of summer insolation and temperature (Meister *et al.* 2024). Despite this, numerous studies have focused on reconstructing Holocene climate, yet continuous, high-resolution $\delta^{18}O_{diatom}$ records—at a decadal scale—are relatively rare for key periods like the HTM. This lack of decadal-resolved data substantially limits our ability to compare rapid modern

climate fluctuations with historical warm periods, such as the Mid-Holocene, and to analyse the impact of modern human activities on lake ecosystems.

In this study, we present a new Holocene $\delta^{18}O_{diatom}$ record from Lake Khamra, eastern Siberia. Our objectives are (i) to investigate the relationship between the Holocene $\delta^{18}O_{diatom}$ record and lake ecosystem development (Baisheva *et al*. 2024) and (ii) to compare our local record with published Northern Hemisphere $\delta^{18}O_{diatom}$ data (Meister *et al*. 2024), to identify common key drivers of $\delta^{18}O_{diatom}$ variability and their operating timescales. Additionally, we provide a new ~210-year continuous multiproxy record from Lake Khamra, covering a phase at the end of the HTM. This record includes $\delta^{18}O_{diatom}$ data, along with carbon, nitrogen, and mercury analyses. It is directly comparable to a recent multiproxy dataset (*c*. 1790–2015 CE) from the same lake (Stieg *et al*. 2024a, b), which captures the modern period of climate warming. Both records, covering approximately 200 years each with a (sub-)decadal mean resolution, were obtained from the same lake system and analysed using identical methods and proxies, allowing a direct comparison. Thus, we aim (iii) to compare proxy variability between a warm phase at the end of the HTM and the modern warm period to assess environmental stability and explore potential human impacts on the lake ecosystem.

Regional setting

Lake Khamra (59.99°N, 112.98°E) is located in the southwest of Yakutia, eastern Siberia (Fig. 1A). The catchment area spans 107.3 km^2 and is surrounded by gentle hills. Situated at an elevation of 340 m above sea level (m a.s.l.), the lake is approximately 30 km northwest of the Lena River. The site is remote, with the nearest settlements, Peleduy and Vitim, situated approximately 40 and 60 km to the southwest of the lake. The lake has a surface area of 4.6 km^2 and reaches a maximum depth of 22.3 m in its centre (Fig. 1B). Hydrologically, the lake is an open system, with a main inflow in the southwest and an outflow in the northeast. Ice and snow cover the lake during winter, as observed during an expedition in March 2020, reaching on average 0.5 m of ice and 1 m of snow at different drilling locations (Biskaborn *et al*. 2021a).

The regional climate is continental, with cold, dry winters and warm, humid summers. Referring to the closest weather station in the settlement of Vitim (European Climate Assessment (ECA) station code: 3235, 59.45°N, 112.58°E, 186 m a.s.l.), the region has a mean annual air temperature of −5.0 °C and an annual precipitation amount of 423 mm (1929–2018 CE). A corresponding climate diagram and further meteorology details are available in Stieg *et al*. (2024b).

The study site is located within the middle taiga (Isaev *et al*. 2010), in the transition zone from evergreen to deciduous needleleaf boreal forest, described in more detail in Glückler *et al*. (2021) and Baisheva *et al*. (2024). According to the observations made in the field, the catchment area is covered by a mixed coniferous forest (Kruse *et al*. 2019; Miesner *et al*. 2022). At a soil depth of 10–20 m, the annual ground temperature ranges between 0 °C and 1 °C (Shestakova *et al*. 2021), characterising discontinuous to sporadic permafrost conditions (Obu *et al*. 2019). In geological terms, the region is underlain by Cambrian bedrock composed of dolomite and limestone, with silty Ordovician sandstone and sporadic clayey Silurian limestone deposits (Chelnokova *et al*. 1988). Lake formation dates back to the Last Glacial Period, and lacustrine conditions were established at around 18.4 cal. ka BP (Baisheva *et al*. 2024).

Material and methods

Sediment core retrieval and corresponding age-depth-model

Two field campaigns, a summer campaign in August 2018 (Kruse *et al*. 2019) and a winter campaign in March 2020 (Biskaborn *et al*. 2021a), were conducted at the lake. This study includes analyses of the sediment short core EN18232-1 from 2018 and the composite long core EN20001 from 2020 (Fig. 1B, Table 1). The composite core EN20001, consisting of six overlapping segments, was recovered using an UWITEC tripod piston coring system from the central part of the lake (59.99095°N, 112.98345°E) at a water depth of 20.6 m (Fig. 1B), while the lake was covered by ice reaching a thickness of up to 65 cm. After retrieval, the core segments were transported to the Alfred Wegener Institute Helmholtz Centre for Polar and Marine Research (AWI), Potsdam, Germany, and split, described and studied for X-Ray fluorescence (XRF) scanning analysis, carbon and nitrogen concentrations, pollen and non-pollen palynomorphs counting, and sedimentary ancient DNA amplicon sequencing of aquatic and terrestrial plants and diatoms (Baisheva *et al*. 2024). Lake level changes discussed in Baisheva *et al*. (2024) were rated using the 'Rarefied sedaDNA diatoms' data provided in their supplementary material, along with habitat assignments from the same publication, by calculating a planktonic to benthic (P/B) ratio, following the methodology outlined in Wang *et al*. (2013). Specifically, the proportion of planktonic diatoms was determined by dividing the sum of all planktonic taxa by the sum of all planktonic and benthic taxa. To highlight the contrast with planktonic species, we grouped epiphytic and benthic taxa.

The corresponding age–depth model was published in detail by Baisheva *et al*. (2024) and is based on 38 radiocarbon dates of bulk sediment samples (Fig. 2A). The study reveals that the record, with a composite depth

Table 1. Overview of sediment cores retrieved from Lake Khamra used in this study, including core ID, core information, location, water depth at the core location, core length, age-depth model details, individual age range and relevant proxy data. The proxy data include diatom oxygen isotope data ($\delta^{18}O_{diatom}$), total mercury (THg), biogeochemical sediment proxies such as total organic carbon (TOC), total nitrogen (TN), their ratio (C/N), as well as their stable isotopes ($\delta^{13}C$ and $\delta^{15}N$), and a planktonic to benthic diatom ratio (P/B ratio) based on diatom sedaDNA analysis. The table highlights both previously published and new data from the cores.

Core ID	Core information	Location	Water depth	Core length	Age information	Age range	Proxy data relevant for this study
EN18232-1 Recent series	Short core; retrieved August 2018	59.99091°N to 112.98373°E	22.3 m	42 cm; continuous samples: 0–39 cm, 1 cm interval	^{210}Pb-^{137}Cs method (Stieg *et al.* 2024b)	2015–1793 CE mean ages, ~220 years, mean age uncertainty ±14 years	$\delta^{18}O_{diatom}$ and THg (Stieg *et al.* 2024b) TOC, TN, C/N, $\delta^{13}C$ and $\delta^{15}N$ (Stieg *et al.* 2024a)
EN20001 Holocene series	Composite long core; retrieved March 2020	59.99095°N, 112.98345°E	20.6 m	Composite depth ~10.8 m	^{14}C method (Baisheva *et al.* 2024)	−0.063-19.604 cal. ka BP mean ages (0–1076 cm)	$\delta^{18}O_{diatom}$, THg and P/B ratio (this study) TOC, TN and C/N (Baisheva *et al.* 2024)
EN20001-6 0–89 cm 6k series	Core segment of EN20001	59.99095°N, 112.98345°E	20.6 m	Upper 22 cm subsampled, 1 cm interval, composite depth 693–714 cm	^{14}C method (Baisheva *et al.* 2024)	6.140–6.347 cal. ka BP mean ages, ~210 years, mean age uncertainty ±110 years	$\delta^{18}O_{diatom}$, THg, TOC, TN, C/N, $\delta^{13}C$ and $\delta^{15}N$ (this study)

of *c.* 10.8 m, dates back to 19.6 cal. ka BP and has its highest sedimentation rate of 0.33 cm a^{-1} at ~5.6 cal. ka BP (Baisheva *et al.* 2024). The calibration is referred to years before present (a BP), where 'present' is 1950 CE. Calibrated age is used in our study.

The sedimentary succession of the core EN20001 is divided into four lithological units (Fig. 2B). The beginning of the Holocene (11.2 cal. ka BP, at 909 cm) lies at the upper end of a unit characterised by a dark-grey, organic-poor mixture of fine and medium-coarse material (1052–892 cm). However, the majority of the Holocene is represented in the upper unit (892–0 cm), which consists of a uniform, dark-brown, organic-rich fine material deposited over the last 10.5 cal. ka BP. The Holocene onset is also supported by diatoms, XRF, and total organic carbon analyses (Baisheva *et al.* 2024). The substantial thickness of approximately 9 m covering the Holocene provides the foundation for decadal-scale studies at Lake Khamra, even in older sediment sections.

Millennial and decadal-scale subsampling of sediment core EN20001

For diatom oxygen isotope determination, 26 subsamples were selected from the composite core EN20001, covering the entire Holocene period and reaching up to 19.6 cal. ka BP, with an average sample resolution of 786 years. The millennial-scale sample series should allow for comparison with other long-term diatom oxygen isotope records from Siberia.

Additionally, we partially subsampled a sediment core segment (EN20001-6, 0–89 cm) of the composite core EN20001 (Table 1). The two radiocarbon dates at the top and base of this segment show no reversal relative to the directly adjacent dates and thus may frame a period with continuous sedimentation (Fig. 2A). This segment was selected due to elevated total organic carbon (TOC) values and a simultaneous maximum in total nitrogen (TN) (Fig. 4B, C; Baisheva *et al.* 2024), which indicate a phase of maximum biological productivity in the lake. Further, the age range of about 6.3–6.1 cal. ka BP identifies a time period at the end of the HTM at Lake Khamra (Baisheva *et al.* 2024), a time with no human impact. Continuous 1-cm slices were extracted from 0 to 22 cm depth downcore (n = 22) to create a diatom oxygen isotope record with decadal resolution, covering about 200 years. The sampling strategy is comparable to a previous study on the short core EN18232-1 of Lake Khamra (Stieg *et al.* 2024b) (Table 1). Subsampling was conducted under sterile conditions in a climate chamber maintained at 4 °C at the German Research Centre for Geosciences (GFZ) in Potsdam. The 1-cm slices were taken parallel to the sediment layers, with the outer rim material (~<0.5 cm) of each subsample being discarded because it touched the plastic of the transport tubes and was likely dragged downward during the coring procedure. The remaining sample material was used for multiproxy analyses, including biogeochemical assessments and mercury concentration determination. This record will be referred to as the '6k series' and serves to compare with a similar sub-decadal record from the same lake, covering the last ~220 years from *c.* 1790 to 2015 CE (Fig. 3A) (Stieg *et al.* 2024b), including the period of the industrial revolution, to analyse the human impact on the hydroclimatic system.

Diatom purification process and contamination assessment

The diatom purification process for isotope analyses involves a combination of chemical and physical prepa-

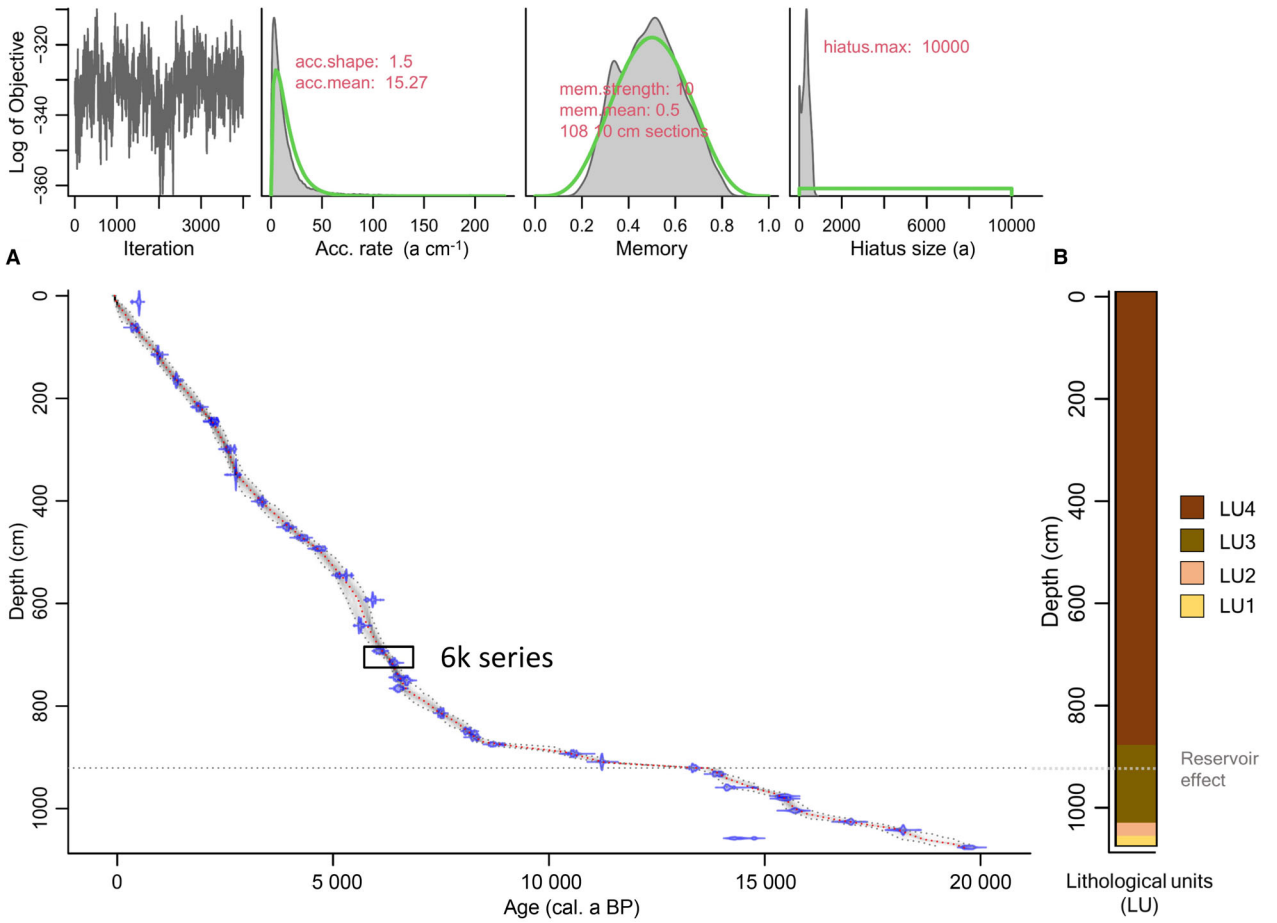

Fig. 2. A. Age-depth model of the core EN20001, first published in Baisheva *et al.* (2024). The age-depth relationship is based on ^{14}C dating of bulk sediment samples (blue signs indicate individual ^{14}C dates, n = 38). The rectangle marks the period of the 6k series. B. Lithology of core EN20001 from Baisheva *et al.* (2024), indicating four lithological units (LU; LU1 = organic-poor, coarse; LU2 = dark organic layers within coarse matrix; LU3 = organic-poor, dark grey, medium coarse; and LU4 = organic-rich, dark brown, fine).

ration techniques to achieve a purified diatom sample (Morley *et al.* 2004; Leng & Barker 2006). The purification steps closely follow the procedure used for previous sediment samples from Lake Khamra, outlined in Stieg *et al.* (2024b), following Morley *et al.* (2004) and Kostrova *et al.* (2021). For processing, we used freeze-dried sample material. Aliquot weights were dependent on the available sample material, averaging 1.5 g for samples of the millennial-scale sample series of the core EN20001 (n = 26) and 1.2 g for the 6k series of the core segment EN20001-6 (n = 22). At the beginning of the purification process, organic matter was removed by using hydrogen peroxide (H_2O_2, 30%) at a temperature of 50 °C for ~55 h, followed by the removal of carbonates with hydrochloric acid (HCl, 10%) for another ~16 h. Subsequently, samples were washed neutral with ultra-pure water to remove any remaining reagents. To separate diatoms from the heavy minerogenic fraction, heavy liquid separations (HLS) were performed by centrifuging the samples with a sodium polytungstate solution (SPT, $3Na_2WO_4{\cdot}9WO_3 \times H_2O$), using specific decreasing densities for the subsamples of EN20001 (2.35–2.15 g cm^{-3}) and the 6k series (2.50–-2.00 g cm^{-3}). Light microparticles, like charcoal, were removed with an inverse HLS, following the procedure described in Kostrova *et al.* (2021). Finally, the purified samples were washed with ultra-pure water through a 1-µm filter to ensure complete neutrality.

We assessed the contamination of each sample to ensure the purity of the prepared diatom samples. A JEOL M-IT500HR analytical scanning electron microscope (SEM) with an integrated energy dispersive X-ray spectroscopy (EDS) system supplied with a Peltier-element-cooled detector (SDD) was applied to identify elements of each sample, given as oxides with weight percentages. Thereby, we followed the standardless procedure, detailed in Chapligin *et al.* (2012a), performing six repetitions with an acceleration voltage of 20.0 kV, a magnification of 300 and a measurement time of 30 s. Aluminium oxide (Al_2O_3) is used as a proxy for the clay fraction and serves as an indicator of sample contamination. Its content should remain below 2.5% to

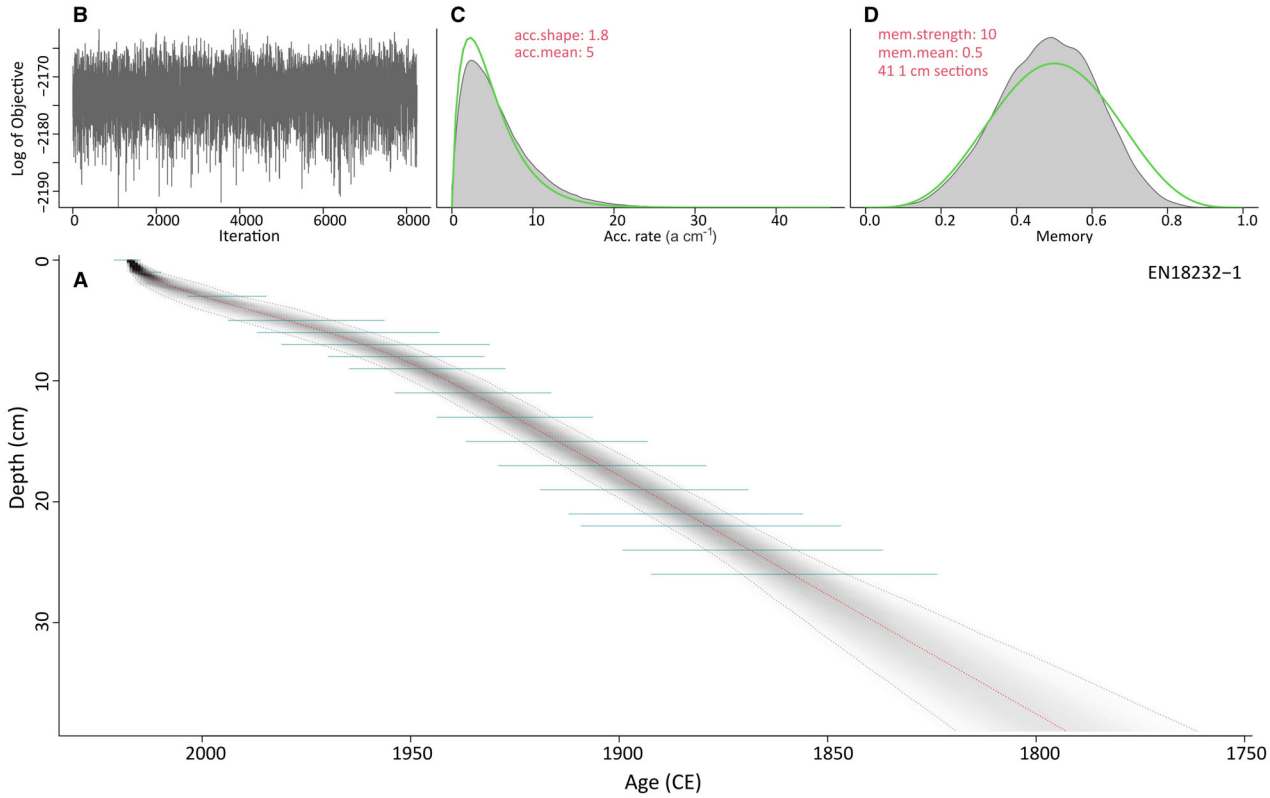

Fig. 3. A. Bayesian accumulation model, first published in Stieg *et al.* (2024b), based on the ^{210}Pb and ^{137}Cs dating (green horizontal lines) of the short core EN18232-1 (dotted grey lines indicate the 2σ range; in red line represents the median). B. Model iteration log. C, D. Prior (green line) and posterior (grey area) distributions for accumulation rate and memory, respectively.

prevent significant shifts due to correction in the diatom oxygen isotope record, while silicon dioxide (SiO_2) reflects the sample's purity (Chapligin *et al.* 2012a).

Diatom oxygen isotope measurements

The diatom oxygen isotope composition was determined using a semi-automated laser-fluorination line (Chapligin *et al.* 2010) at the ISOLAB Facility at AWI Potsdam, coupled with a Sercon HS2022 mass spectrometer. Prior to measurements, we applied the inert gas flow dehydration method (iGFD; Chapligin *et al.* 2010), heating up aliquots of the processed sample material with ramp degassing at up to 1100 °C under an inert (either Argon or Helium) gas flow to remove exchangeable hydroxyl groups from the siliceous diatom cell walls. During the laser fluorination, oxygen was quantitatively released using bromine pentafluoride (BrF_5) as a reagent (Clayton & Mayeda 1963).

The oxygen isotope composition was determined relative to reference material with a known isotopic value, expressed in delta notation ($\delta^{18}O_{diatom}$) relative to VSMOW in per mil (‰). As laboratory standards, we used BFC 2 ($\delta^{18}O$ = +27.63±0.22‰, n = 34) and PS Jun17_2 ($\delta^{18}O$ = +43.84±0.28‰, n = 16), both calibrated against the marine standard PS1772-8 and the biogenic silica standard BFC (Chapligin *et al.* 2010, 2011). Additionally, BDP-1 (fossil lacustrine diatoms) was established as a new laboratory control standard ($\delta^{18}O$ = +27.11±0.27‰, n = 43). Its accuracy and analytical precision are comparable to the method's long-term analytical reproducibility (1σ) of ±0.25‰ (Chapligin *et al.* 2010).

All $\delta^{18}O_{diatom}$ measurements were adjusted for contamination using the geochemical mass-balance approach (Brewer *et al.* 2008; Swann & Leng 2009; Chapligin *et al.* 2012a), following the same procedure as described in Stieg *et al.* (2024b).

Mercury analyses

Total mercury concentration (THg) was determined in 43 subsamples from the composite core EN20001 (Table 1), in addition to the existing biogeochemical analyses (TOC, TN, and C/N; details in Baisheva *et al.* 2024), to determine the background signal of the lake sediment. Furthermore, THg was analysed in 22 subsamples from the 6k series (EN20001-6) to provide comparative values with recent sediment samples of the short core EN18232-1 (Table 1). Due to lim-

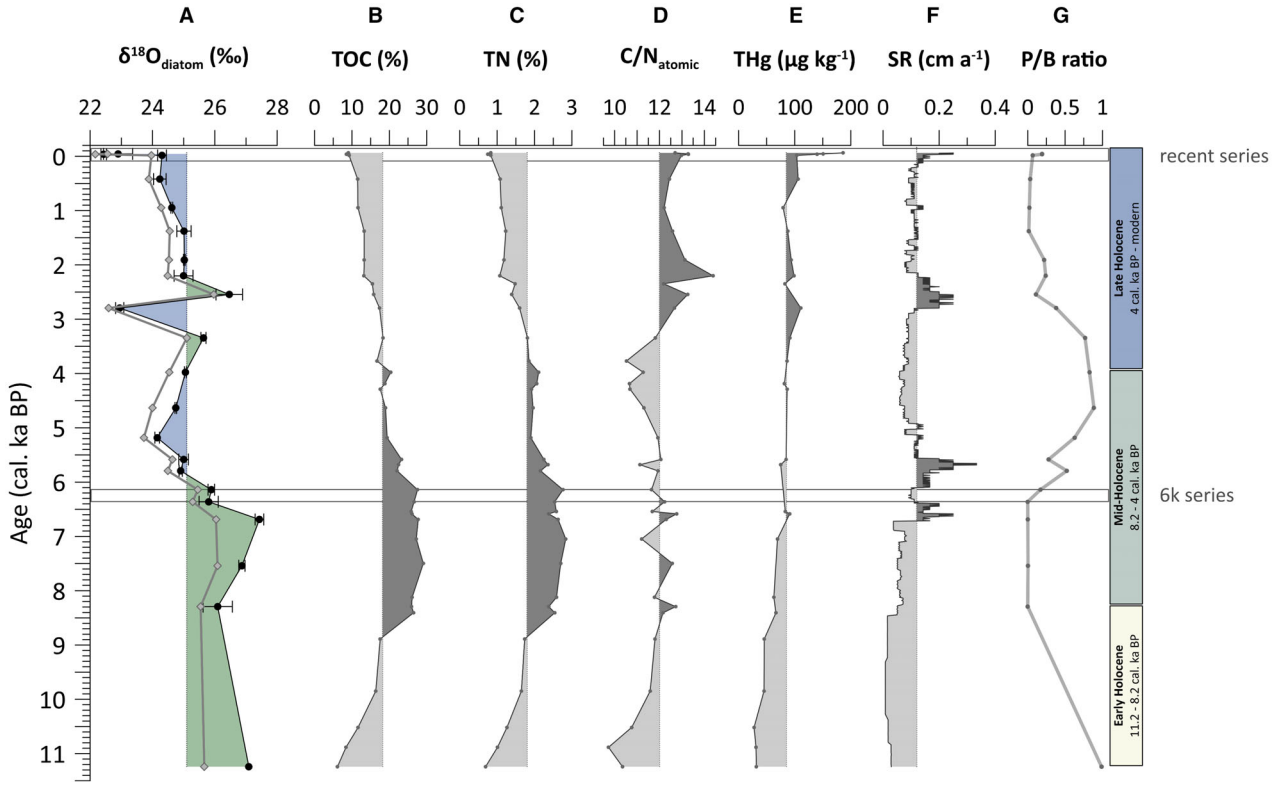

Fig. 4. A. Holocene $\delta^{18}O_{diatom}$ record of the core EN20001 from Lake Khamra, black circles indicate corrected $\delta^{18}O_{diatom}$ values, grey diamonds show values before contamination correction. B.–F. Lake-internal parameters (TOC, TN, C/N and SR; Baisheva *et al.* 2024) of core EN20001. E. Mercury concentrations (THg) of core EN20001. The shading of the individual curves indicates values above or below the individual mean. G. Planktonic to benthic (P/B) ratio based on 'Rarefied sedaDNA diatoms' data published in Baisheva *et al.* (2024). Horizontal bars highlight the period of the recent sample series of the short core EN18232-1 (*c.* 1790–2015 CE) and the 6k series of core segment EN20001-6 (*c.* 6.140–6.350 cal. ka BP). The division into Early-, Mid- and Late Holocene is based on the study of Baisheva *et al.* (2024).

ited sample material, THg in the 6k series was analysed from the rim material. THg concentrations (µg kg^{-1}) were measured using an MLS-MWS DMA-80 evo III at the BioGeoChemistry Laboratory, AWI Potsdam. The instrument had a detection limit of 0.003 ng, with a laboratory-established limit of determination of 0.4 ng.

Biogeochemical proxies (TOC, TN, $\delta^{13}C$ and $\delta^{15}N$) of the 6k series

TOC and TN concentrations of the 6k series samples (n = 21; EN20001-6) were measured to examine variations in the organic matter content of the lake sediments, in comparison with the recent sediment samples of Lake Khamra (Table 1). Before analysis, freeze-dried aliquots were ground in an agate mill to achieve a uniform sample material. TOC was assessed using an Elementar soli TOC cube, while TN was determined with an Elementar rapid MAX N exceed. Both instruments provided a measurement accuracy of 0.1%, and analyses were performed at the BioGeoChemistry Laboratory at AWI Potsdam. The atomic TOC/TN ratio (C/N), which serves as an indicator of the organic matter source, was calculated by multiplying the mass ratio by 1.167, which is the atomic-weight ratio of carbon to nitrogen (Meyers & Teranes 2001).

Stable carbon isotope ratios ($^{13}C/^{12}C$) were determined to gain further insights into past productivity and organic matter sources, in relation to the recent Lake Khamra sediments. Before isotope analysis, inorganic carbon was removed using a 1.3 mol L^{-1} hydrochloric acid (HCl) treatment on freeze-dried and milled samples (n = 21). The carbon isotope measurements were conducted at the ISOLAB at AWI Potsdam using a ThermoFisher Scientific Delta-V-Advantage gas mass spectrometer, integrated with a FLASH EA 2000 elemental analyser, a CONFLO IV gas-mixing system and an MA200R autosampler. Results are calibrated against laboratory standards with known isotopic compositions and referenced to the Vienna Pee Dee Belemnite (VPDB) standard. Nitrogen isotope ratios ($^{15}N/^{14}N$) of 21 samples were determined using the same gas mass spectrometer. Results are presented relative to the standard atmospheric nitrogen ratio (air). Both carbon and nitrogen isotope ratios are expressed in delta notation ($\delta^{13}C$, $\delta^{15}N$) in per mil (‰), with standard errors of less than ±0.15‰ (1σ).

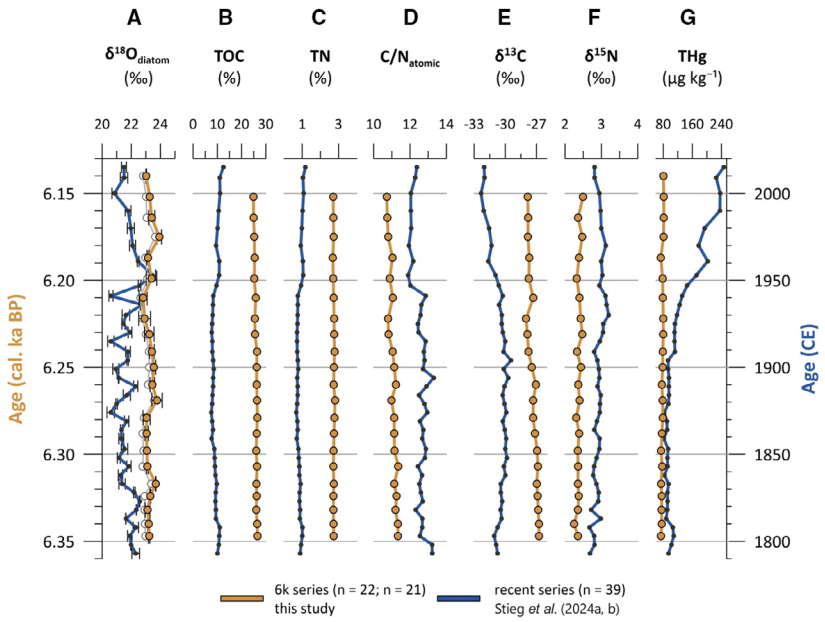

Fig. 5. A. $\delta^{18}O_{diatom}$ record of the 6k series (core segment EN20001-6), with the uncorrected record displayed in grey. B.–F. Biogeochemical parameters and mercury concentrations (G) of the 6k series. Data from the recent series (EN18232-1), first published in Stieg *et al.* (2024a, b) are integrated for comparison and coloured in blue, using the same proxies.

Comparison of decadal multiproxy records of Lake Khamra

We compared the decadal multiproxy datasets from the 6k series (EN20001-6) with the recent record from Lake Khamra, which is derived from analyses of the parallel short core EN18232-1 (Fig. 1B, Table 1), focusing on differences in absolute values and their variability. Proxy data of the recent dataset are available online via the PANGAEA database; the specific dataset links are provided in the Data Availability Statement. The proxies used for comparison include $\delta^{18}O_{diatom}$, TOC, TN, C/N, $\delta^{13}C$, $\delta^{15}N$, and mercury concentrations. Boxplots are used to illustrate the differences between the datasets and to visualise variability.

Results

Millennial and decadal-scale Holocene diatom oxygen isotope records

The millennial-scale series contained 26 samples, of which only 22 could be sufficiently purified for isotope measurement (mean Al_2O_3 = 0.7%, mean SiO_2 = 98.7% and n = 22). The oldest four samples (≥14.680 cal. ka BP) contained too few diatoms for the purification process and the subsequent isotope measurement. The remaining 22 samples were measured at least twice, except for the oldest sample of the record (*c.* 11.240 cal. ka BP), for which there was only sufficient material for one measurement. The series will be referred to as the 'Holocene record'. Overall, the Holocene $\delta^{18}O_{diatom}$ record has a mean of +25.1‰, with a standard deviation (SD) of ±1.3‰ and a total range of ±5‰. The mean analytical reproducibility of the sample material was 0.17‰, with a maximum of 0.47‰. Contamination correction increased all measurements by an average of +0.5‰, with a minimum increase of +0.3‰ and a maximum of +1.4‰ (Fig. 4A). Across the entire Holocene record, we observe a negative trend of −0.3‰ ka^{-1}. Between about 11.2 and 6.7 cal. ka BP, the Holocene $\delta^{18}O_{diatom}$ record reveals the most elevated values, starting with a maximum of +27.1‰ at 11.2 cal. ka BP and including the total maximum of +27.4‰ at about 6.7 cal. ka BP (Fig. 4A). Thereafter, $\delta^{18}O_{diatom}$ values decline stepwise by about −3.2‰ until +24.2‰ at 5.2 cal. ka BP. Following, the $\delta^{18}O_{diatom}$ record slightly increases again and establishes a rather stable phase around or slightly below the mean until −0.016 cal. ka BP, with high variability between 3.3 and 2.5 cal. ka BP, which includes a minimum of +22.9‰ at 2.8 cal. ka BP. The most recent two samples of the record, past −0.016 cal. ka BP, show a drastic drop of nearly −2‰, including the total minimum of +22.4‰ at −0.038 cal. ka BP (Fig. 4A).

The 6k series spans the time period from about 6.140 to 6.350 cal. ka BP (mean ages), resulting in a decadal mean sampling resolution of 9.9±1.6 years (min: 7, max: 12 years). All 22 samples of the 6k series were successfully processed and purified for the oxygen isotope measurements (mean Al_2O_3 = 0.4%, mean SiO_2 = 99.1%, n = 22). Each sample was measured at least twice. Contamination correction increased all diatom $\delta^{18}O$ values by an average of +0.3‰ (Fig. 5A), with a maximum correction of +0.4‰ and a minimum of

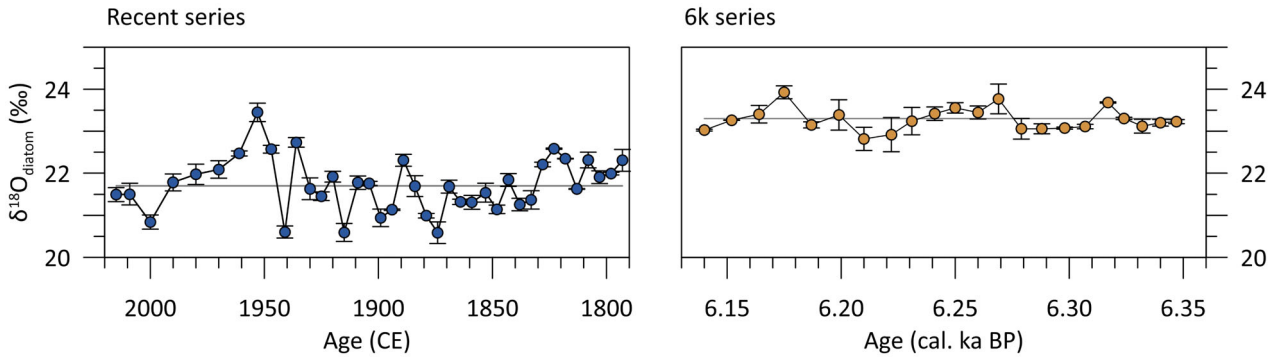

Fig. 6. Recent $\delta^{18}O_{diatom}$ record of the short core EN18232-1 (Stieg *et al.* 2024b) compared to $\delta^{18}O_{diatom}$ record of the 6k series of the core segment EN20001-6 of Lake Khamra. Horizontal lines indicate the individual mean value. Both x-axes cover a time span of 230 years and share the same scaling to ensure comparability.

+0.2‰. These corrections are identical to the purity and the minimal corrections of the recent $\delta^{18}O_{diatom}$ series of Lake Khamra (Stieg *et al.* 2024b). The $\delta^{18}O_{diatom}$ values of the 6k series have an overall mean of +23.3±0.3‰ (n = 22), indicating isotopic enrichment compared to the recent series (Figs 5A, 6), which has a mean value of +21.7±0.6‰ (n = 39) and a total range of 2.9‰ (Stieg *et al.* 2024b). In the 6k series, values range from a minimum of +22.8‰ at ~6.210 cal. ka BP to a maximum of +23.9‰ at ~6.175 cal. ka BP (Fig. 6), reflecting a narrower total range of 1.1‰ (Table 2). The analytical reproducibility of the sample material was consistently ≤0.41‰ and generally (with five exceptions) ≤0.25‰.

Both, the recent and 6k series, show slightly more depleted $\delta^{18}O_{diatom}$ values compared to the corresponding parts of the Holocene record. These differences are likely related to the sampling of different sediment cores or core segments (Table 1). However, both the recent and the Holocene records display similar trends of more depleted values in the most recent samples, which supports their overall reliability. To account for the discrepancy, we focus on general trends and rates of change for the millennial-scale Holocene record and use the two high-resolution series for comparing decadal-scale variabilities.

Mercury concentrations of the Holocene

All mercury measurements (n = 43) of the composite core EN20001 are above the detection limit of 0.003 ng. In the Holocene, THg has a mean value of 85 μg kg^{-1} (n = 27). Between *c.* 11.2 and 4 cal. ka BP, THg remains below the Holocene mean and rises from 32 to 82 μg kg^{-1}. Thereafter, THg continues to increase until modern times up to 104 μg kg^{-1} (−0.016 cal. ka BP). In the most recent three samples, we identify a drastic increase up to 186 μg kg^{-1} in the youngest sample. We show the THg measurements along with the Holocene $\delta^{18}O_{diatom}$ record and other lake internal parameters such as TOC, TN, C/N, and sedimentation rates (SR) from Baisheva *et al.* (2024) (Fig. 4A–F). Additionally, we integrate the results of the P/B ratio, derived from the 'Rarefied sedaDNA diatoms' dataset (Baisheva *et al.* 2024), into this lake internal plot (Fig. 4G). The P/B ratio has a mean value of 0.3 for the period 11.2 to −0.044 cal. ka BP (mean ages, n = 22), with values ranging from 0 to 0.99.

In subsamples of the 6k series, THg levels range from a minimum of 73.4 μg kg^{-1} to a maximum of 81.4 μg kg^{-1} (Fig. 5G), remaining close to the mean of 77.6 μg kg^{-1} (n = 22).

Carbon and nitrogen proxies of 6k series

Overall, the biogeochemical proxies of the 6k series exhibit relatively low variability throughout the record (Fig. 5B–F). TOC averages 25.9% (n = 21), with a maximum of 26.5% at *c.* 6.350 cal. ka BP and a minimum of 24.9% at *c.* 6.150 cal. ka BP. TN remains largely stable around its mean of 2.7% (n = 21). The C/N ratio declines slightly towards the younger samples, similar to TOC (Fig. 5B, D), to a minimum of 10.7 in the uppermost sample (*c.* 6.150 cal. ka BP), with an overall mean of 11.1 (n = 21). $\delta^{13}C$ and $\delta^{15}N$ values also indicate low variability (Fig. 5E, F). $\delta^{13}C$, with a mean of −27.3‰ (n = 21), ranging from a minimum of −28.0‰ around 6.220 cal. ka BP to a maximum of −26.8‰ in the three oldest samples downcore. $\delta^{15}N$ has a mean of 2.4‰ (n = 21) and shows minor variability with a SD of ±0.1‰.

The comparison between the 6k series and the recent dataset of the short core EN182321 (Table 1) is summarised in Table 2 and shown in Fig. 5, while Fig. 8 visualises differences in absolute values and variability using box plots.

Discussion

Modern hydrology and drivers of diatom oxygen isotopes at Lake Khamra

A comprehensive understanding of the modern hydrology of the study site and the drivers influencing $\delta^{18}O_{diatom}$ is essential for accurate interpretation of the

Table 2. Comparison of key statistics, including mean, median, standard deviation (SD), minimum (Min), maximum (Max) and total range (Max –Min), for the comparable proxies of the recent ('Recent') and 6k series ('6k').

	Mean		Median		SD		Min		Max		Total range	
	Recent	6k	Recent	6k	Recent	6k	Recent	6k	Recent	6k	Recent	6k
$\delta^{18}O_{diatom}$ (‰)	21.7	23.3	21.7	23.2	0.6	0.3	20.6	22.8	23.4	23.9	2.9	1.1
TOC (%)	9.2	25.9	9	26.1	1.2	0.5	7.5	24.9	12.5	26.5	5	1.6
TN (%)	0.9	2.7	0.8	2.7	0.1	0	0.7	2.7	1.2	2.8	0.5	0.1
C/N	12.6	11.1	12.6	11.1	0.3	0.2	11.9	10.7	13.3	11.4	1.4	0.6
$\delta^{13}C$ (‰)	−30.6	−27.3	−30.3	−27.3	0.7	0.4	−32.3	−28	−29.5	−26.8	2.9	1.2
$\delta^{15}N$ (‰)	2.9	2.4	2.9	2.4	0.1	0.1	2.7	2.2	3.2	2.5	0.5	0.2
THg (μg kg^{-1})	123	77.6	95.8	78.4	48.8	2.6	81.7	73.4	246.3	81.4	164.6	8

oxygen isotope signatures of lacustrine diatoms (Leng & Barker 2006). The hydrology of Lake Khamra, along with the water isotopic composition and its relationship to the $\delta^{18}O_{diatom}$ in modern sediment samples, was thoroughly examined in a previous study (Stieg *et al.* 2024b). Key findings indicate that Lake Khamra represents an open lake system, whose lake water isotope signature is generally linked to that of the precipitation ($\delta^{18}O_{prec}$) (Leng & Barker 2006). In the region, $\delta^{18}O_{prec}$ exhibits a strong seasonality related to monthly air temperatures (T_{air}) changes, with enriched values during summer and strongly depleted values in the cold season, with a high seasonal variation $\Delta^{18}O$ of up to 22‰ (based on stable isotope data of Yakutsk; Kurita *et al.* 2004). Modern snow samples revealed the lowest isotopic signatures (mean $\delta^{18}O = -29.14 \pm 0.5$‰, $n = 2$; Stieg *et al.* 2024b), underlining these observations. Using the OIPC (Online Isotopes in Precipitation Calculator; Bowen 2024), we calculated a modern modelled annual mean of $\delta^{18}O_{prec}$ of −13.2‰ for the study site (latitude 60°, longitude 113°, altitude 340 m a.s.l.; Bowen & Revenaugh 2003; IAEA/WMO 2015; Bowen 2024). Overall, depleted oxygen isotopes of the lake water (mean $\delta^{18}O_{lake}$, March 2020: −19.98±0.14‰; $n = 6$; Stieg *et al.* 2024b) compared to the modelled annual mean of $\delta^{18}O_{prec}$ suggest that Lake Khamra is influenced by isotopically light precipitation. As there are no glaciers in the region and the area lies only within a discontinuous to sporadic permafrost zone (Obu *et al.* 2019; Shestakova *et al.* 2021), which could both contribute isotopically depleted waters through melting or degradation, we assume the lake is primarily fed by snow and snowmelt. Although evaporation might occur during summer months, its effect on $\delta^{18}O_{lake}$ is considered minimal. This is indicated by the lake water isotopes being positioned close to the global and local meteoric water lines in the co-isotope plot (Stieg *et al.* 2024b). In addition, a persistent ice cover for over 6 months each year and the lake's approximately annual mixing (residence time: 474 days; Messager *et al.* 2016) further limit the impact of evaporation.

Based on the most recent $\delta^{18}O_{diatom}$ of +22.9‰ at −0.044 cal. ka BP of the Holocene record and the mean $\delta^{18}O_{lake}$ (−19.98‰), we estimate a water temperature of approximately +4.2 °C using the equation of isotopic fractionation of Leclerc & Labeyrie (1987). This estimate closely aligns with the previously calculated temperature range of +4.8 to +8.7 °C (Stieg *et al.* 2024b) based on data from the short core EN18232-1 (Table 1), which is realistic for the early summer months shortly after the ice break-up. It also falls within the growth temperature range of *Aulacoseira subarctica* (4–16 °C; Gibson *et al.* 2003), the dominant diatom species in the recent record (Stieg *et al.* 2024a), supporting the reliability of the new $\delta^{18}O_{diatom}$ record.

Oxygen isotope composition in diatom silica is influenced by both direct and indirect factors, leading to an increase or decrease of the isotopic signature during fractionation processes, as compiled in Meister *et al.* (2024). The key factors here are the temperature-dependent fractionation during biosynthesis (~−0.2‰ per °C; Moschen *et al.* 2005; Dodd & Sharp 2010), which contrasts with the positive temperature-dependent fractionation of the oxygen isotopes in precipitation. The latter influences the isotopic signature of the lake water ($\delta^{18}O_{lake}$). Globally, the temperature-dependent fractionation of precipitation amounts to +0.7‰ per °C (Dansgaard 1964), though it is even stronger at Lake Khamra using local meteorological and modelled data (+0.8‰ per °C; Stieg *et al.* 2024b). Consequently, at Lake Khamra, the influence of T_{air} on the $\delta^{18}O_{diatom}$ variability surpasses that of lake temperature (T_{lake}) during biosynthesis, as shown in many other diatom isotope studies of the Northern Hemisphere (e.g. Meyer *et al.* 2015a; Chapligin *et al.* 2016; Broadman *et al.* 2022). As outlined, the influence of winter precipitation, specifically isotopically depleted snow meltwater, has been identified as the primary factor influencing $\delta^{18}O_{lake}$ and, as a consequence, the diatom isotope variability over the recent $\delta^{18}O_{diatom}$ record of Lake Khamra. According to this, low $\delta^{18}O_{diatom}$ values were interpreted as increased inflow of isotopically light $\delta^{18}O$ snow meltwater, while high $\delta^{18}O_{diatom}$ values were associated with reduced inflow. Rising air temperatures and solar radiation, however, could be largely ruled out as primary drivers for the recent $\delta^{18}O_{diatom}$ record, as their trends run opposite to the diatom oxygen isotopes (Stieg *et al.* 2024b).

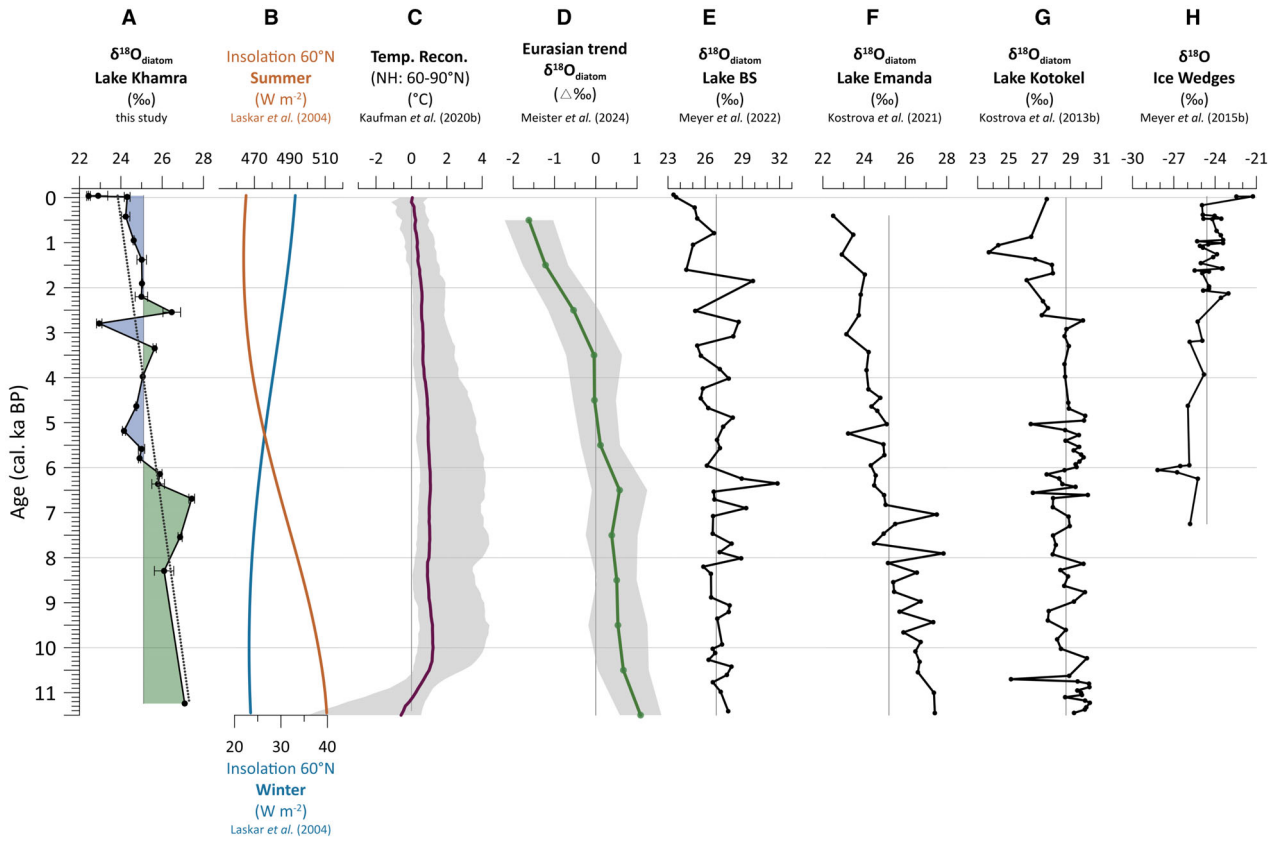

Fig. 7. A. Holocene $\delta^{18}O_{diatom}$ record of Lake Khamra with an individual trend line indicating negative Holocene trend of $-0.3‰\ ka^{-1}$; the shading indicates values above or below the individual mean. B.–H. External proxies. B. Summer and winter insolation calculated for 60°N (Laskar *et al.* 2004). C. Proxy-based temperature reconstruction for 60–90°N (Kaufman *et al.* 2020). D. Compilation of Eurasian $\delta^{18}O_{diatom}$ records (Meister *et al.* 2024). E.–G. Selected $\delta^{18}O_{diatom}$ records: Towards the west from Lake Khamra in the Polar Urals, Lake Bolshoye Shchuchye (Lake BS) (Meyer *et al.* 2022); eastern Siberia, Lake Emanda (Kostrova *et al.* 2021); southern Siberia, Lake Kotokel close to Lake Baikal (Kostrova *et al.* 2013b). H. $\delta^{18}O$ record of permafrost ice wedges from the Lena River delta used as a winter temperature proxy (Meyer *et al.* 2015b).

Millennial-scale isotopic changes in relation to lake-internal parameters during the Holocene

During the Holocene, the Lake Khamra $\delta^{18}O_{diatom}$ record indicates a decreasing trend ($-0.3‰\ ka^{-1}$; $n = 22$) (Fig. 4A) and the mean value (+25.1‰) falls within the general range of Northern Hemisphere $\delta^{18}O_{diatom}$ records (mean values between +20‰ and +35‰; Meister *et al.* 2024). During the Early and Mid-Holocene (11.2 to 6 cal. ka BP), $\delta^{18}O_{diatom}$ values remain above the Holocene average (Fig. 4A), with two maxima at 11.2 and 6.7 cal. ka BP. According to the interpretation of the recent series from Lake Khamra (Stieg *et al.* 2024b), elevated $\delta^{18}O_{diatom}$ values would signify either a decreased influence of isotopically light snow meltwater or warmer T_{air}. The climate during the Early Holocene at Lake Khamra is described as warmer and wetter than that of the Late Pleistocene (Baisheva *et al.* 2024). At the onset of the $\delta^{18}O_{diatom}$ record at about 11.2 cal. ka BP, lake bioproductivity significantly increased at Lake Khamra, identified by rising total organic carbon (TOC; Fig. 4B) and Bromine values (Br; shown in Baisheva *et al.* 2024). The temperature rise led to the establishment of taiga forest and overall denser vegetation around Lake Khamra. This contributed to increased TOC and reduced erosional input (Baisheva *et al.* 2024), as evidenced by low sedimentation rates (SR) until approximately 6.7 cal. ka BP (Fig. 4F). The strongly positive link between T_{air} and $\delta^{18}O_{prec}$ at the study site suggests that warmer conditions likely contributed to elevated values of $\delta^{18}O_{lake}$, and consequently $\delta^{18}O_{diatom}$, as observed in our record. The $\delta^{18}O_{diatom}$ record does not cover the transition from the Late Pleistocene to the Holocene. However, the maximum in $\delta^{18}O_{diatom}$ at 11.2 cal. ka BP might also be linked to particularly high T_{air}, which represents one of the highest temperatures within the Holocene, especially at its onset (Fig. 7C). A reduced snowmelt influx during the Early Holocene as an explanation for elevated $\delta^{18}O_{diatom}$ values seems rather unlikely, as tendentially more melting would be expected during a warming phase.

Until 6.7 cal. ka BP, the diatom isotope record is still characterised by relatively high $\delta^{18}O_{diatom}$ values, consistently remaining above the Holocene mean (Fig. 4A). At

11.2 cal. ka BP, marking the onset of the Holocene, a shift in diatom species composition towards planktonic species occurred (Fig. 4G), including *Aulacoseira* (Baisheva *et al*. 2024). This shift has been interpreted as a rise in lake water level, while low C/N ratios, as an indicator of organic matter source (Meyers & Teranes 2001), suggest a more distal and algae-dominated environment (Baisheva *et al*. 2024). A wetter climate at the onset of the Holocene at Lake Khamra (Baisheva *et al*. 2024) could have contributed to higher $\delta^{18}O_{lake}$ and, consequently, $\delta^{18}O_{diatom}$ values if driven by isotopically enriched summer precipitation, alongside rising air temperatures. Nevertheless, the resolution at the onset of the isotope record is limited, making it challenging to draw explicit conclusions.

The $\delta^{18}O_{diatom}$ maximum at 6.7 cal. ka BP (Fig. 4A) coincides with the highest bioproductivity, indicated by a maximum in TOC (Fig. 4B) and Br between 8.2 and 6 cal. ka BP (Baisheva *et al*. 2024). The presence of diatom taxa indicating warm conditions (Baisheva *et al*. 2024) suggests that elevated temperatures played a key role in both lake productivity and elevated $\delta^{18}O_{diatom}$ during the Mid-Holocene. A decrease in planktonic diatoms from 8.2 to 6.5 cal. ka BP (Fig. 4G) indicates lower lake levels at Lake Khamra (Baisheva *et al*. 2024). Combined with elevated temperatures, this could have led to enhanced evaporative effects, which have the potential to further increase the $\delta^{18}O_{diatom}$ values (Meister *et al*. 2024). The presence of *Abies sibirica* and *Larix sibirica* in the sedaDNA record of Lake Khamra at 6.3 cal. ka BP (Baisheva *et al*. 2024) was interpreted to be representative of permafrost degradation (Tchebakova *et al*. 2009) and low winter temperatures as well as reduced precipitation (Pelánková *et al*. 2008), further reinforcing the idea that over the Mid-Holocene, warmer and drier conditions led to high $\delta^{18}O_{diatom}$ values.

After the maximum of $\delta^{18}O_{diatom}$ at 6.7 cal. ka BP, $\delta^{18}O_{diatom}$ decreased stepwise until 5.2 cal. ka BP, coinciding with a reported lake level rise at around 6.5 cal. ka BP (Baisheva *et al*. 2024), which is reflected in the increase of planktonic diatom taxa in the P/B ratio (Fig. 4G). At the same time, the SR increases and displays high variability framing the 6k series (Fig. 4F). The high SR and simultaneously occurring age reversals in the ^{14}C dating (Baisheva *et al*. 2024) (Fig. 2A) could also indicate mass wasting processes, potentially triggered by increased precipitation and enhanced erosional input. The stepwise decline in the $\delta^{18}O_{diatom}$ record after its maximum at 6.7 cal. ka BP could be related to reduced evaporation effects during higher precipitation levels, an increase in precipitation primarily from isotopically lighter winter precipitation entering the lake as depleted snow meltwater, as well as a decrease in air temperature. A more abrupt climatic cooling in the Lake Khamra region has been suggested only after *c*. 4.5 cal. ka BP, indicated by a decline in warm-water diatom species and macrophytes (Baisheva *et al*. 2024). However, the $\delta^{18}O_{diatom}$ values show a modest but continuous increase of +1.4‰ after the minimum at 5.2 cal. ka BP, continuing until 3.3 cal. ka BP (Fig. 4A). This suggests that the cooling inferred from the biological proxies after approximately 4.5 cal. ka BP is not directly reflected in the $\delta^{18}O_{diatom}$ record, as the trends are opposing.

After 3.3 cal. ka BP, the $\delta^{18}O_{diatom}$ record indicates increased variability between 2.8 and 2.2 cal. ka BP, coinciding with another SR maximum (Fig. 4F). At the same time, C/N rises and reaches its absolute Holocene maximum at 2.2 cal. ka BP, suggesting a potentially increased input of organic matter from terrestrial plants, even though it displays a mixed-source signal between aquatic and land origin (Meyers & Teranes 2001). This could indicate another period of increased precipitation and erosional input, driving centennial-scale variability in the $\delta^{18}O_{diatom}$ record.

A charcoal record from Lake Khamra (Glückler *et al*. 2021) reveals the regional wildfire history over the last approximately 2200 years. In the recent $\delta^{18}O_{diatom}$ record of the short core EN18232-1, charcoal maxima coincide with elevated $\delta^{18}O_{diatom}$ values and were associated with possible dry periods characterised by reduced winter precipitation and, consequently, a decreased inflow of isotopically lighter snow meltwater (Stieg *et al*. 2024b). Referring to the charcoal record (Glückler *et al*. 2021), periods of increased fire activity are indicated between 600 and 900 CE (1.350 and 1.050 cal. ka BP) and after 1750 CE (0.200 cal. ka BP). In the Holocene $\delta^{18}O_{diatom}$ record, we observe a continuous decrease in $\delta^{18}O_{diatom}$ from around 1.5 cal. ka BP, with no signs of higher variability during periods of increased fire frequency. However, the resolution of the Holocene record limits the detection of fire-induced short-term fluctuations on these timescales.

After −0.016 cal. ka BP, we observe a drastic $\delta^{18}O_{diatom}$ decrease of approximately −2‰, including the absolute minimum of +22.4‰ at −0.038 cal. ka BP. These $\delta^{18}O_{diatom}$ values approach the recent Khamra record, which has an average value of +21.7‰, strongly influenced by isotopically light winter precipitation (Stieg *et al*. 2024b). Simultaneously, SR again shows a maximum during this recent period (Fig. 4F), further supporting the idea of precipitation-driven $\delta^{18}O_{diatom}$ variability on centennial scales.

Thus, in comparison with other lake-internal parameters, the Holocene $\delta^{18}O_{diatom}$ record of Lake Khamra appears to follow temperature changes over millennial timescales. Especially in the Early to Mid-Holocene, elevated $\delta^{18}O_{diatom}$ values align with interpretations of the lake development, likely indicating warmer conditions during a period of high bioproductivity. However, the stepwise decline in the $\delta^{18}O_{diatom}$ record at Lake Khamra, beginning after 6.7 cal. ka BP until 5.2 cal. ka BP, could be linked to decreasing temperatures and increasing precipitation levels. Since biological lake-

internal proxies indicate a shift to colder conditions only from 4.5 cal. ka BP onwards, the $\delta^{18}O_{diatom}$ decline here appears to be more closely associated with increased precipitation, which is also reflected in the rising lake level, as indicated by the increasing P/B ratio. High centennial-scale variability in the $\delta^{18}O_{diatom}$ record corresponds with increased sedimentation rates during the Mid- and Late Holocene. This suggests that fluctuations in precipitation likely influenced $\delta^{18}O_{diatom}$ signal, potentially overlaying the broader cooling trend over the Holocene.

Diatom oxygen isotope patterns at Lake Khamra in the Northern Hemisphere and Eurasian context

In the recent decadal-scale $\delta^{18}O_{diatom}$ series, isotopically light winter precipitation acts as a key influence on $\delta^{18}O_{lake}$, and consequently, on $\delta^{18}O_{diatom}$. At millennial timescales, we hypothesise that $\delta^{18}O_{diatom}$ at Lake Khamra is primarily influenced by summer climate variations, following a long-term decreasing summer insolation and air temperature trend throughout the Holocene (Fig. 7A–C). Similar Holocene $\delta^{18}O_{diatom}$ trends have been observed in other Eurasian lake studies (e.g. Swann *et al.* 2010; Mackay *et al.* 2011; Chapligin *et al.* 2012b; Kostrova *et al.* 2013b, 2021).

In a compilation of lacustrine $\delta^{18}O_{diatom}$ records (Fig. 7D), Meister *et al.* (2024) presented a stack of Northern Hemisphere data, revealing a common pattern that clearly aligns with the long-term decrease of summer insolation and air temperature throughout the Holocene. The decreasing Holocene trend observed at Lake Khamra ($-0.3‰$ ka^{-1}; $n = 22$; Fig. 7A) is in the same range, but slightly stronger than the decrease observed in the compiled $\delta^{18}O_{diatom}$ records from hydrologically open lakes with water residence times under 100 years across the Northern Hemisphere ($-0.19‰$ ka^{-1}) and Eurasia ($-0.21‰$ ka^{-1}), respectively (Meister *et al.* 2024). The statistical combination of individual records into a common trend likely led to a flattening of the trend compared to the values from a single record. The negative trend at Lake Khamra is comparable to, for example, the $\delta^{18}O_{diatom}$ decrease observed further northeast, at Lake Emanda (Figs 1A, 7F; Kostrova *et al.* 2021).

At Lake Khamra, the highest $\delta^{18}O_{diatom}$ values occur during the Early to Mid-Holocene between 11.2 and 6.7 cal. ka BP, which align well with an overall summer insolation maximum at 60°N (Fig. 7B; Laskar *et al.* 2004). Simultaneously at the onset of the Holocene, the Northern Hemisphere experienced a rapid warming (Fig. 7C; Kaufman *et al.* 2020). The positive air temperature-dependent fractionation of precipitation at the study site (+0.8‰ per °C; Stieg *et al.* 2024b) suggests that warmer conditions likely contributed to elevated $\delta^{18}O_{lake}$, and hence $\delta^{18}O_{diatom}$. An increased summer insolation could have enhanced evaporation during the ice-free season at Lake Khamra, which would further contribute to higher $\delta^{18}O_{diatom}$ values. However, based on the findings of Baisheva *et al.* (2024), the rise in planktonic diatoms (Fig. 4G), along with higher lake levels and moisture conditions at the beginning of the Holocene, suggests that evaporative effects were likely minimal. This supports the interpretation that elevated $\delta^{18}O_{diatom}$ values were primarily driven by summer insolation and warmer temperatures, rather than by evaporation. Winter insolation can be largely discounted as a potential driver of $\delta^{18}O_{diatom}$ at Lake Khamra on millennial timescales. Winter and summer insolation show opposing trends throughout the Holocene, with winter insolation remaining generally low and indicating a minimum at the beginning of the Holocene (Fig. 7B; Laskar *et al.* 2004). Additionally, reconstructed winter temperatures, as indicated by a $\delta^{18}O$ record of permafrost ice wedges from the Lena River Delta (Figs. 1A, 7H; Meyer *et al.* 2015b), have generally increased since the Mid- to Late Holocene, opposite to the decreasing Holocene $\delta^{18}O_{diatom}$ record. This suggests that the long-term $\delta^{18}O_{diatom}$ trend is rather linked to the summer season, coinciding with the main diatom bloom that occurs from late spring to early summer, shortly after the ice break-up.

In the diatom isotope compilation by Meister *et al.* (2024), Holocene maxima of Eurasian records regionally differ. While eastern Eurasian sites show an earlier Holocene maximum around 12 cal. ka BP, western Eurasian sites display a later maximum, occurring during the Mid-Holocene between 8 and 6 cal. ka BP (Meister *et al.* 2024). Accordingly, the Lake Khamra $\delta^{18}O_{diatom}$ record aligns more closely with the eastern study sites, revealing its first maximum at the onset of the record at 11.2 cal. ka BP. However, this maximum should be interpreted cautiously as it relies on a single measurement and due to enhanced contamination corrections, particularly in the older section of the core (Fig. 4A). Nevertheless, consistently elevated values during the Early Holocene, including a second maximum around 6.7 cal. ka BP, share similarities with the Lake Emanda record in northeastern Siberia, which also reveals high $\delta^{18}O_{diatom}$ at both the beginning and during the Mid-Holocene (Fig. 7F). The timing of the absolute $\delta^{18}O_{diatom}$ maximum at 6.7 cal. ka BP at Lake Khamra could be linked to the HTM, which is generally associated with the maximum of summer solar insolation. At the same time, we also observe a maximum in the lake's bioproductivity (Baisheva *et al.* 2024), as illustrated by the maxima in TOC and TN, supporting the interpretation of a warm and insolation-rich period at Lake Khamra. The alignment of the Lake Khamra record with the general Eurasian trend (Fig. 7D; Meister *et al.* 2024) suggests that it is consistent with broader Eurasian summer temperature and insolation trends during the Holocene. However, the timing of the HTM varies both spatially and temporally across the Northern Hemisphere (Kaufman 2004; Renssen *et al.* 2009), which is

also reflected in different spatiotemporal patterns observed in northeastern Siberia (Biskaborn *et al*. 2016) and evidenced by the individual maxima in $\delta^{18}O_{diatom}$ records from the Northern Hemisphere stack (Meister *et al*. 2024).

After 6.7 cal. ka BP, the $\delta^{18}O_{diatom}$ values decline stepwise until 5.2 cal. ka BP, reaching a minimum which is also noted at Lake Emanda (Kostrova *et al*. 2021). The authors attributed this depletion to a distinct cooling event with global implications, driven by prolonged positive North Atlantic Oscillation (NAO) conditions (Roland *et al*. 2015). This event around 5.2 ka BP might also be reflected in the Khamra record, as the recent $\delta^{18}O_{diatom}$ data suggest a possible relationship with the NAO, indicating the transport of moisture via the westerlies, which impacts the hydroclimate at Lake Khamra (Stieg *et al*. 2024b).

We attributed the centennial-scale variability after 3.3 and 2.2 cal. ka BP to precipitation variability, as discussed in relation to the lake-internal parameters. At Lake Kotokel, close to Lake Baikal (Fig. 1A), high variability in $\delta^{18}O_{diatom}$ is observed after 2.7 cal. ka BP (Fig. 7G), linked to a decrease in precipitation and a temperature decline in the region (Tarasov *et al*. 2007; Kostrova *et al*. 2013b). Also, at Lake Emanda, a minimum at 3 cal. ka BP is recorded (Fig. 7F), seen as regional cooling (Kostrova *et al*. 2021). Focusing on the long-term trends on millennial scales, other Northern Hemisphere and especially Eurasian records also show a clear decrease following the Mid-Holocene optimum (Fig. 7D). However, the decline in the compiled Eurasian records is rather later compared to the Lake Khamra record, and starts only at 4 cal. ka BP (Meister *et al*. 2024). This decrease of $\delta^{18}O_{diatom}$ on the Northern Hemisphere has been linked to a phenomenon known as Neoglacial cooling, with decreasing summer temperatures in the Arctic and an associated advance of Northern Hemisphere glaciers (Solomina *et al*. 2015). The temporal offset in the decreasing trend of the Khamra record compared to the compiled $\delta^{18}O_{diatom}$ records (Meister *et al*. 2024) could result from a smoothing effect inherent in data compilation, which can obscure individual record trends. Alternatively, it suggests that the Lake Khamra record behaves similarly to eastern Eurasian sites that closely follow the insolation curve as a proxy for summer air temperature (Chapligin *et al*. 2012b; Kostrova *et al*. 2021; Meister *et al*. 2024), which declines even earlier (Fig. 7B).

Over the last 1–2 cal. ka BP, the decrease in Khamra's $\delta^{18}O_{diatom}$ aligns well with the decline of the Eurasian compilation (Fig. 7D; Meister *et al*. 2024). Nevertheless, further climatic events of the Northern Hemisphere cannot be clearly verified due to the multi-centennial resolution of the Khamra Holocene record. The recent drastic decrease in $\delta^{18}O_{diatom}$ values at Lake Khamra after −0.016 cal. ka BP mirrors similar trends in other Eurasian records, such as Lake Bolshoye Shchuchye in the Polar Urals (Figs 1A, 7E; Meyer *et al*. 2022), where a Holocene $\delta^{18}O_{diatom}$ minimum contrasts with the current global temperature rise. Meyer *et al*. (2022) also noted a shift in key drivers on $\delta^{18}O_{diatom}$ at Lake Bolshoye Shchuchye, with millennial-scale trends following decreasing summer insolation and temperatures, while short-term variations are linked to snowmelt variability (Fig. 7E), similar to the interpretation of the recent $\delta^{18}O_{diatom}$ Khamra record (Stieg *et al*. 2024b).

Throughout the Holocene, the Lake Khamra diatom oxygen isotope record is driven by large-scale factors, generally aligning with millennial-scale trends of declining summer insolation and corresponding changes in air temperature. The $\delta^{18}O_{diatom}$ record from Lake Khamra shares strong similarity with the Eurasian trends, particularly those from sites in eastern Eurasia, such as Lake Emanda (Kostrova *et al*. 2021).

Decadal-scale multiproxy comparison of Mid-Holocene and recent warm phases at Lake Khamra

In order to assess the potential impacts of human activity on the lake ecosystem, we compare two warm periods recorded in the sediment cores of Lake Khamra, the end of the HTM (6k series) and the recent climate warming (recent series) (Table 1). During the HTM, both TOC and TN reach their highest levels (Fig. 4B, C), indicating a productivity maximum at Lake Khamra between 8.2 and 6 cal. ka BP (Baisheva *et al*. 2024). In the broader context of global climate, the HTM is characterised by global mean surface temperatures approximately 0.7 °C higher than in the preindustrial era (Kaufman *et al*. 2020). In comparison, the recent Khamra record (*c*. 1790–2015 CE; Stieg *et al*. 2024b) covers the modern climate warming. We hypothesise that human influence might have increased the variability in the recent proxy records compared to the natural warming phase of the Mid-Holocene, which occurred without anthropogenic impacts, thereby reflecting effects of human activity on hydroclimatic systems.

Boxplots of the two multiproxy records reveal notable differences not only in total values but also in variability (Fig. 8), highlighting contrasts between the two warm phases at Lake Khamra. The median $\delta^{18}O_{diatom}$ value in the recent series (median: +21.7‰) is 1.5‰ lower than those of the 6k series (median: +23.2‰, see Table 2). As previously discussed, the $\delta^{18}O_{diatom}$ values primarily followed the solar insolation and air temperatures during the Holocene, with the highest $\delta^{18}O_{diatom}$ values during the Early and Mid-Holocene. In contrast, the recent series is strongly influenced by winter precipitation, which reaches the lake through isotopically lighter meltwater inflow, explaining the lower $\delta^{18}O_{diatom}$ values despite the recent rise in air temperatures (Stieg *et al*. 2024b). Notably, the standard deviation in the recent series (+21.7±0.6‰) is twice as high as in the 6k series (+23.3±0.3‰). Additionally, the total range of

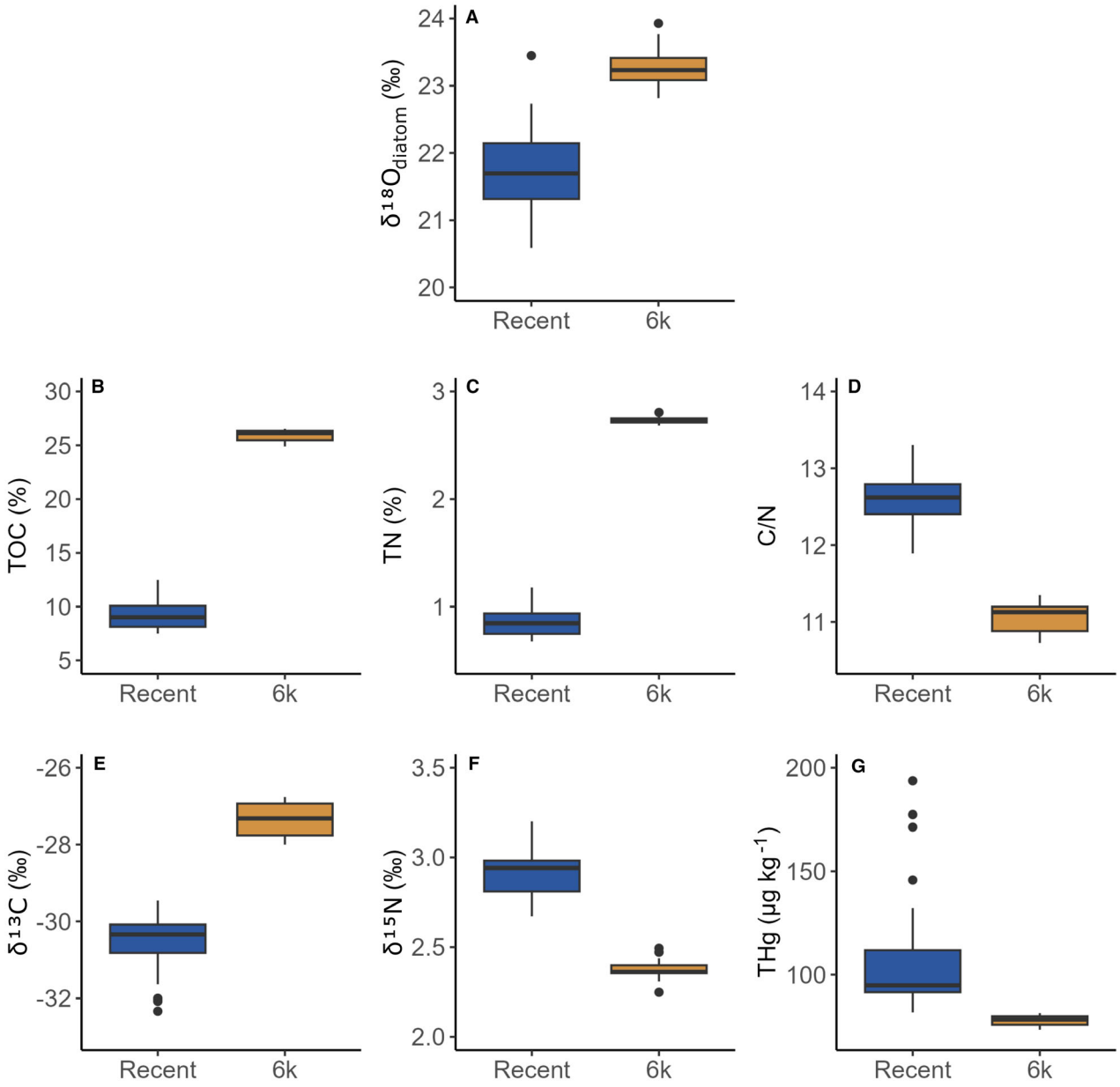

Fig. 8. Boxplots of individual proxies from the recent series (short core EN18232-1, blue, Stieg *et al.* 2024a, b) and the 6k series (core segment EN20001-6, orange) of Lake Khamra. Proxies include diatom oxygen isotope data ($\delta^{18}O_{diatom}$), total organic carbon (TOC), total nitrogen (TN), their ratio (C/N), as well as their stable isotopes ($\delta^{13}C$, $\delta^{15}N$) and total mercury (THg) (A–G). The boxplots illustrate differences in central tendency, variability, and outliers for each parameter.

variability in the recent series (2.9‰) is nearly three times greater than that of the 6k series (1.1‰; Table 2, Fig. 8A). This suggests that, although both periods were characterised as warm phases, the recent series shows greater variability (Fig. 6), likely driven by increased hydroclimatic fluctuations, while conditions during the ~200-year period of the 6k series were probably more stable at Lake Khamra. Besides hydroclimate changes, differential signal preservation and smoothing, such as by bioturbation or diffusive processes, might have affected both datasets differently, though these aspects lie beyond the scope of this study. Moreover, the $\delta^{18}O_{diatom}$ values of the 6k series could potentially be influenced by long-term diagenetic processes, which could elevate the original isotope values (Meister *et al.* 2024). However, analysis from a 250 ka record of Lake El'gygytgyn in the Far East Russian Arctic (Fig. 1A) indicates no significant trend towards higher $\delta^{18}O$ values, suggesting that diagenetic effects on $\delta^{18}O_{diatom}$ are rather minimal (Chapligin *et al.* 2012b).

TOC and TN serve as indicators of organic matter content and are closely linked to primary productivity (Meyers & Teranes 2001). According to Baisheva *et al.* (2024), bioproductivity reached its Holocene max-

imum between 8.2 and 6 cal. ka BP, followed by a decline towards the Late Holocene. This decreasing trend is clearly illustrated when comparing the two high-resolution records. Compared to TOC in the 6k series, the carbon content in the recent series decreased by a factor of 2.8, while TN values dropped to about one-third (Fig. 8B, C, Table 2). The recent series also demonstrates greater variability in TOC and TN, evident in the higher standard deviations and increased total ranges (Table 2). Furthermore, a tendency towards higher values in the recent series has been observed since the 1950s, corroborated by rising carbon accumulation rates since the 1970s, interpreted as a rise in productivity (Stieg *et al.* 2024a). However, despite this recent rise in productivity, the recent TOC and TN values remain well below the maximum levels recorded during the end of the HTM (Fig. 8B, C).

The C/N ratios of both series indicate no distinct source signal of organic matter (Fig. 8D), consistent with observations from the Holocene sediment record on a millennial scale (Fig. 4D). This suggests contributions from both aquatic sources and terrestrial plants (Meyers & Teranes 2001). However, a lower C/N ratio from the 6k series suggests a tendency towards a higher proportion of aquatic productivity, in contrast to the recent series. This aligns with the observations made by Baisheva *et al.* (2024), suggesting the occurrence of epiphytic and benthic taxa and a lake expansion with colonisation of the lake periphery in the Mid-Holocene. Nevertheless, the recent series shows a greater total range (Table 2), possibly indicating larger fluctuations in organic matter sources over similar time periods. This could be linked to higher variability between reduced and increased erosional input from snowmelt inflow in recent times, which is also reflected in the rapidly rising SR in recent times (Fig. 4F). In contrast, the 6k series is framed by maxima in SR rates, but the period itself displays more stable SR (Fig. 4F). Bordered by two radiocarbon dates, the 6k period shows no age reversals and maintains a continuous age-depth relationship (Fig. 2A), which indicates more stable conditions characterised by high internal lake productivity compared to the recent series.

Potential anthropogenic effects on Lake Khamra sediments could be inferred from the $\delta^{13}C$, $\delta^{15}N$, and mercury concentration data. Algae and terrestrial plants have indistinguishable $\delta^{13}C$ values, with both $\delta^{13}C$ records falling within the typical range of −31 to −25‰ (Meyers 2009). However, recent series show lighter $\delta^{13}C$ (−30.6±0.7‰) compared to the 6k series (−27.3±0.4‰), with a median difference of 3‰ and outliers towards even lighter values (Fig. 8E). This depletion in the recent series has been partially attributed to a potential anthropogenic imprint resulting from fossil fuel combustion (Stieg *et al.* 2024a), known as the *Suess effect* (Keeling 1979), as seen, for example, in lake sediment records from Greenland (Stevenson *et al.* 2021). The higher $\delta^{13}C$ values in the 6k series could reflect increased aquatic productivity at the end of the HTM, as enhanced productivity is associated with rising $\delta^{13}C$ values in organic matter (Meyers 2009). This period falls within a peak of bioproductivity that occurred between 8.2 and 6 cal. ka BP, as outlined in Baisheva *et al.* (2024). However, $\delta^{13}C$ values in sediments are influenced by multiple factors, and besides bioproductivity, source changes, and the decomposition of organic matter, other (post-depositional) processes, such as changes in bottom-water redox conditions over time, could also have contributed to the observed difference in $\delta^{13}C$.

The $\delta^{15}N$ values in both series (Fig. 8F) indicate a mixed source signal from algae (5–10‰) and terrestrial sources (around 0‰; Meyers 2009), similar to the C/N ratios. Even though differences are small, the recent series exhibit slightly higher $\delta^{15}N$ values than the 6k series (Table 2), which is somewhat unexpected. Human activities, such as fossil fuel combustion and fertiliser production, are a man-made source of reactive nitrogen (Nr) (Galloway *et al.* 2008) with lighter isotopic $\delta^{15}N$ released into the atmosphere, which affects lake systems globally and has led to the deposition of anthropogenic depleted $\delta^{15}N$ in lake sediments (Holtgrieve *et al.* 2011; McLauchlan *et al.* 2013; Wolfe *et al.* 2013). Given that Lake Khamra, despite its remote location, is suggested to be influenced by atmospheric pollution (Stieg *et al.* 2024b), we would have expected lower $\delta^{15}N$ values compared to the 6k series. However, nitrogen isotope fractionation processes (Meyers & Teranes 2001) and diagenetic processes in the sediment are complex, and it appears that not all lakes show a recent decline in $\delta^{15}N$ values, depending on nitrogen inputs and the in-lake N pool (Anderson *et al.* 2018). Furthermore, $\delta^{15}N$ in lake sediments displays a natural variability throughout the Holocene, with a decline until the Mid-Holocene, followed by an increase thereafter (McLauchlan *et al.* 2013). This variability could be evident in the comparison of the two periods at Lake Khamra, which does not indicate any anthropogenic $\delta^{15}N$ depletion in recent times.

In contrast to the $\delta^{15}N$ data, the changes in THg in the sediment samples are more pronounced, suggesting a link to human influence. Although the median THg values of both series are relatively close (Table 2, Fig. 8G), the recent series shows a much higher range, with values reaching up to 246.3 μg kg^{-1}. We calculated a baseline level of THg in Lake Khamra sediments over the Holocene prior to industrial times (>1850 CE) of 74.7 μg kg^{-1} (n = 23), which is quite comparable to the median of the 6k series (Table 2). The increase in THg concentrations in recent times, also reflected in the recent spike in the Holocene record (Fig. 4E), was partially attributed to far-reaching anthropogenic inputs from fossil fuel combustion and air pollution, particularly since the 1990s, due to industrialisation in Asia (Stieg *et al.* 2024b).

The multiproxy comparison shows that the 6k series is rather stable with minimal fluctuations, while the recent series, despite both representing warm phases, exhibits greater variability and different absolute values (Figs 5, 8). Elevated aquatic productivity and stable hydroclimatic conditions during the 6k period likely explain the consistency, while the increased variability and divergent values in the recent series are attributed to greater hydroclimatic fluctuations, which are contemporaneous with human influence on the lake ecosystem.

Conclusions

The new Holocene $\delta^{18}O_{diatom}$ record from Lake Khamra in eastern Siberia enhances our understanding of the proxy's seasonal and long-term dynamics during the Holocene. It offers insights into the hydroclimatic development in Yakutia, thereby enhancing the regional coverage across Siberia. The $\delta^{18}O_{diatom}$ record aligns well with interpretations of the lake ecosystem development based on published biodata of the same sediment core. Elevated $\delta^{18}O_{diatom}$ values during the Early to Mid-Holocene correspond to a period of high bioproductivity and warmer air temperatures.

In contrast to the recent sub-decadal $\delta^{18}O_{diatom}$ record for the past ~220 years, which is influenced by isotopically light winter precipitation, the Holocene $\delta^{18}O_{diatom}$ record over millennial timescales generally follows a long-term decline in summer insolation and the associated decrease in air temperatures in the Northern Hemisphere. Higher variability observed on a centennial scale in the Holocene $\delta^{18}O_{diatom}$ record corresponds to phases with increased sedimentation rates, likely driven by fluctuations in precipitation that overprint the general temperature trend. The overall decreasing Holocene trend in $\delta^{18}O_{diatom}$ aligns with findings from other Eurasian lake studies. Furthermore, the $\delta^{18}O_{diatom}$ shows strong similarities with eastern Eurasian sites, suggesting a regional Early Holocene maximum. In particular, the resemblance to Lake Emanda suggests a broader regional hydroclimatic pattern.

A new decadal multiproxy record from Lake Khamra (6k series), covering a *c*. 210-year period during the Mid-Holocene, has been compared to a recent sub-decadal dataset from the same lake. Both analysed periods occur within warm phases, at the end of the HTM and the recent warming. The multiproxy comparison reveals that the 6k series is notably more stable, with minimal fluctuations across the proxy records. In contrast, the analysed parameters in the recent record not only differ in their absolute values but also indicate consistently higher variability. These observations reflect an increased recent hydroclimatic variability and a potential human impact, as suggested by mercury and $\delta^{13}C$ signatures in organic matter. The multiproxy comparison enhances our understanding of hydroclimate variability over the Holocene and provides deeper insights into the lake ecosystem development.

Acknowledgements. – We thank the teams of the ISOLAB Facility and the BioGeoChemistry lab of the AWI in Potsdam. Special thanks go to Izabella Baisheva for her assistance with sub-sampling the sediment core, as well as to all participants of the joint German–Russian expeditions in Yakutia in 2018 and 2020 for their valuable contributions. We also thank the guest editor Juliane Müller, the referee Bernd Wagner and an anonymous reviewer for their constructive comments and valuable suggestions, which helped to improve the manuscript. Amelie Stieg is funded by AWI INSPIRES (International Science Program for Integrative Research in Earth Systems). We acknowledge support by the Open Access publication fund of the AWI. Open Access funding enabled and organized by Projekt DEAL.

Author contributions. – AS, HM, BKB and UH developed the research project. BKB, UH and LP conducted fieldwork in 2018 and 2020 and received the sediment core. AS subsampled the core segment, processed and analysed the sediment samples in the lab and, together with HM, interpreted the diatom isotope datasets. SK processed the newly introduced laboratory diatom isotope control standard. JS supervised the biogeochemical and mercury analysis and helped interpret these proxies. AS and HM structured the manuscript. AS produced all figures and tables, and wrote the manuscript. All authors reviewed and commented on the text and approved the final version. All authors are free of competing interests.

Data availability statement. – The data presented in this study are accessible through the PANGAEA database as follows:

Holocene series:

- Stieg, Amelie; Marent, Andreas; Weiner, Mikaela; Biskaborn, Boris K; Herzschuh, Ulrike; Baisheva, Izabella; Pestryakova, Luidmila A; Meyer, Hanno (2025): Holocene diatom oxygen isotope record from Lake Khamra, Yakutia, Siberia [dataset]. PANGAEA, https://doi.org/10.1594/PANGAEA.973013.
- Biskaborn, Boris K; Stieg, Amelie; Stoof-Leichsenring, Kathleen Rosmarie; Baisheva, Izabella; Strauss, Jens; Lindemann, Justin; Pestryakova, Luidmila A; Herzschuh, Ulrike (2025): Mercury concentrations of sediment core EN20001 of Lake Khamra, Yakutia, Siberia [dataset]. PANGAEA, https://doi.org/10.1594/PANGAEA.973014.

6k series:

- Stieg, Amelie; Weiner, Mikaela; Marent, Andreas; Biskaborn, Boris K; Herzschuh, Ulrike; Baisheva, Izabella; Pestryakova, Luidmila A; Meyer, Hanno (2025): Decadal diatom oxygen isotope record of the Mid-Holocene (ca. 6.140–6.347 cal. ka BP) of the sediment core segment EN20001_6 from Lake Khamra, Yakutia, Siberia [dataset]. PANGAEA, https://doi.org/10.1594/PANGAEA.973010.
- Stieg, Amelie; Weiner, Mikaela; Strauss, Jens; Lindemann, Justin; Biskaborn, Boris K; Herzschuh, Ulrike; Baisheva, Izabella; Pestryakova, Luidmila A; Meyer, Hanno (2025): Carbon and nitrogen concentrations alongside stable isotopes of the sediment core segment EN20001_6 from Lake Khamra, Yakutia, Siberia [dataset]. PANGAEA, https://doi.org/10.1594/PANGAEA.973011.
- Stieg, Amelie; Strauss, Jens; Lindemann, Justin; Biskaborn, Boris K; Herzschuh, Ulrike; Baisheva, Izabella; Pestryakova, Luidmila A; Meyer, Hanno (2025): Mercury concentrations of the EN20001_6 core segment from Lake Khamra, Yakutia, Siberia [dataset]. PANGAEA, https://doi.org/10.1594/PANGAEA.973012.

Recent series:

- Stieg, Amelie; Biskaborn, Boris K; Herzschuh, Ulrike; Strauss, Jens; Pestryakova, Luidmila A; Meyer, Hanno (2024): Sub-decadal diatom oxygen isotope record and biogeochemical data of the last

220 years (2015–1790CE) based on a sediment short core from Lake Khamra, Yakutia, Siberia [dataset bundled publication]. PANGAEA, https://doi.org/10.1594/PANGAEA.962988.

- Stieg, Amelie; Biskaborn, Boris K; Herzschuh, Ulrike; Strauss, Jens; Lindemann, Justin; Meyer, Hanno (2025): Biogeochemical proxies of the sediment short core EN18232-1, Lake Khamra, Siberia [dataset]. PANGAEA, https://doi.org/10.1594/PANGAEA.971277.

References

Anderson, N. J., Curtis, C. J., Whiteford, E. J., Jones, V. J., McGowan, S., Simpson, G. L. & Kaiser, J. 2018: Regional variability in the atmospheric nitrogen deposition signal and its transfer to the sediment record in Greenland lakes. *Limnology and Oceanography 63*, 2250–2265. https://doi.org/10.1002/lno.10936.

Andreev, A. A., Nazarova, L. B., Lenz, M. M., Böhmer, T., Syrykh, L., Wagner, B., Melles, M., Pestryakova, L. A. & Herzschuh, U. 2022: Late Quaternary paleoenvironmental reconstructions from sediments of Lake Emanda (Verkhoyansk Mountains, East Siberia). *Journal of Quaternary Science 37*, 884–899. https://doi.org/10.1002/jqs.3419.

Baisheva, I., Biskaborn, B. K., Stoof-Leichsenring, K. R., Andreev, A., Heim, B., Meucci, S., Ushnitskaya, L. A., Zakharov, E. S., Dietze, E., Glückler, R., Pestryakova, L. A. & Herzschuh, U. 2024: Late Glacial and Holocene vegetation and lake changes in SW Yakutia, Siberia, inferred from sedaDNA, pollen, and XRF data. *Frontiers in Earth Science 12*, 1354284. https://doi.org/10.3389/feart.2024.1354284.

Baisheva, I., Pestryakova, L., Levina, S., Glückler, R., Biskaborn, B. K., Vyse, S. A., Heim, B., Herzschuh, U. & Stoof-Leichsenring, K. R. 2023: Permafrost-thaw lake development in Central Yakutia: sedimentary ancient DNA and element analyses from a Holocene sediment record. *Journal of Paleolimnology 70*, 95–112. https://doi.org/10.1007/s10933-023-00285-w.

Baumer, M. M., Wagner, B., Meyer, H., Leicher, N., Lenz, M., Fedorov, G., Pestryakova, L. A. & Melles, M. 2020: Climatic and environmental changes in the Yana highlands of north-eastern Siberia over the last c. 57 000 years, derived from a sediment core from Lake Emanda. *Boreas 50*, 114–133. https://doi.org/10.1111/bor.12476.

Biskaborn, B. K., Bolshiyanov, D., Grigoriev, M. N., Morgenstern, A., Pestryakova, L. A., Tsibizov, L. & Dill, A. 2021a: Russian-German cooperation: expeditions to Siberia in 2020. *In Berichte zur polar- und Meeresforschung = reports on polar and marine research*. 87 pp. Alfred Wegener Institute for Polar and Marine Research, Bremerhaven. https://doi.org/10.48433/BzPM_0756_2021.

Biskaborn, B. K., Herzschuh, U., Bolshiyanov, D., Savelieva, L. & Diekmann, B. 2012: Environmental variability in northeastern Siberia during the last ~ 13,300 yr inferred from lake diatoms and sediment–geochemical parameters. *Palaeogeography, Palaeoclimatology, Palaeoecology 329-330*, 22–36. https://doi.org/10.1016/j.palaeo.2012.02.003.

Biskaborn, B. K., Herzschuh, U., Bolshiyanov, D., Savelieva, L., Zibulski, R. & Diekmann, B. 2013: Late Holocene thermokarst variability inferred from diatoms in a lake sediment record from the Lena Delta, Siberian Arctic. *Journal of Paleolimnology 49*, 155–170. https://doi.org/10.1007/s10933-012-9650-1.

Biskaborn, B. K., Narancic, B., Stoof-Leichsenring, K. R., Pestryakova, L. A., Appleby, P. G., Piliposian, G. T. & Diekmann, B. 2021b: Effects of climate change and industrialization on Lake Bolshoe Toko, eastern Siberia. *Journal of Paleolimnology 65*, 335–352. https://doi.org/10.1007/s10933-021-00175-z.

Biskaborn, B. K., Nazarova, L., Kröger, T., Pestryakova, L. A., Syrykh, L., Pfalz, G., Herzschuh, U. & Diekmann, B. 2021c: Late quaternary climate reconstruction and Lead-lag relationships of biotic and sediment-geochemical indicators at Lake Bolshoe Toko, Siberia. *Frontiers in Earth Science 9*, 737353. https://doi.org/10.3389/feart.2021.737353.

Biskaborn, B. K. and 47 others 2019: Permafrost is warming at a global scale. *Nature Communications 10*, 264. https://doi.org/10.1038/s41467-018-08240-4.

Biskaborn, B. K., Subetto, D. A., Savelieva, L. A., Vakhrameeva, P. S., Hansche, A., Herzschuh, U., Klemm, J., Heinecke, L., Pestryakova, L. A., Meyer, H., Kuhn, G. & Diekmann, B. 2016: Late quaternary vegetation and lake system dynamics in north-eastern Siberia: implications for seasonal climate variability. *Quaternary Science Reviews 147*, 406–421. https://doi.org/10.1016/j.quascirev.2015.08.014.

Bowen, G. J. 2024: The online isotopes in precipitation calculator, version OIPC3.1. Available at: http://www.waterisotopes.org (accessed 20.09.2024).

Bowen, G. J. & Revenaugh, J. 2003: Interpolating the isotopic composition of modern meteoric precipitation. *Water Resources Research 39*, 1299. https://doi.org/10.1029/2003WR002086.

Brewer, T. S., Leng, M. J., Mackay, A. W., Lamb, A. L., Tyler, J. J. & Marsh, N. G. 2008: Unravelling contamination signals in biogenic silica oxygen isotope composition: the role of major and trace element geochemistry. *Journal of Quaternary Science 23*, 321–330. https://doi.org/10.1002/jqs.1171.

Broadman, E., Kaufman, D. S., Anderson, R. S., Bogle, S., Ford, M., Fortin, D., Henderson, A. C. G., Lacey, J. H., Leng, M. J., McKay, N. P. & Muñoz, S. E. 2022: Reconstructing postglacial hydrologic and environmental change in the eastern Kenai Peninsula lowlands using proxy data and mass balance modeling. *Quaternary Research 107*, 1–26. https://doi.org/10.1017/qua.2021.75.

Chapligin, B., Leng, M. J., Webb, E., Alexandre, A., Dodd, J. P., Ijiri, A., Lücke, A., Shemesh, A., Abelmann, A., Herzschuh, U., Longstaffe, F. J., Meyer, H., Moschen, R., Okazaki, Y., Rees, N. H., Sharp, Z. D., Sloane, H. J., Sonzogni, C., Swann, G. E. A., Sylvestre, F., Tyler, J. J. & Yam, R. 2011: Inter-laboratory comparison of oxygen isotope compositions from biogenic silica. *Geochimica et Cosmochimica Acta 75*, 7242–7256. https://doi.org/10.1016/j.gca.2011.08.011.

Chapligin, B., Meyer, H., Bryan, A., Snyder, J. & Kemnitz, H. 2012a: Assessment of purification and contamination correction methods for analysing the oxygen isotope composition from biogenic silica. *Chemical Geology 300–301*, 185–199. https://doi.org/10.1016/j.chemgeo.2012.01.004.

Chapligin, B., Meyer, H., Friedrichsen, H., Marent, A., Sohns, E. & Hubberten, H. W. 2010: A high-performance, safer and semi-automated approach for the δ18O analysis of diatom silica and new methods for removing exchangeable oxygen. *Rapid Communications in Mass Spectrometry 24*, 2655–2664. https://doi.org/10.1002/rcm.4689.

Chapligin, B., Meyer, H., Swann, G. E. A., Meyer-Jacob, C. & Hubberten, H. W. 2012b: A 250 ka oxygen isotope record from diatoms at Lake El'gygytgyn, far east Russian Arctic. *Climate of the Past 8*, 1621–1636. https://doi.org/10.5194/cp-8-1621-2012.

Chapligin, B., Narancic, B., Meyer, H. & Pienitz, R. 2016: Paleoenvironmental gateways in the eastern Canadian Arctic – Recent isotope hydrology and diatom oxygen isotopes from Nettilling Lake, Baffin Island, Canada. *Quaternary Science Reviews 147*, 379–390. https://doi.org/10.1016/j.quascirev.2016.03.028.

Chelnokova, S. M., Chikina, I. D. & Radchenko, S. A. 1988: Geologic Map of Yakutia P-48,49, 1 : 1000000, VSEGEI, Leningrad. Available at: http://www.geokniga.org/sites/geokniga/ (accessed 11.11.2022).

Clayton, R. N. & Mayeda, T. K. 1963: The use of bromine pentafluoride in the extraction of oxygen from oxides and silicates for isotopic analysis. *Geochimica et Cosmochimica Acta 27*, 43–52. https://doi.org/10.1016/0016-7037(63)90071-1.

Courtin, J., Andreev, A. A., Raschke, E., Bala, S., Biskaborn, B. K., Liu, S., Zimmermann, H., Diekmann, B., Stoof-Leichsenring, K. R., Pestryakova, L. A. & Herzschuh, U. 2021: Vegetation changes in Southeastern Siberia during the Late Pleistocene and the Holocene. *Frontiers in Ecology and Evolution 9*, 625096. https://doi.org/10.3389/fevo.2021.625096.

Czerniawska, J. & Chlachula, J. 2020: Climate-change induced permafrost degradation in Yakutia, East Siberia. *Arctic 73*, 509–528. https://doi.org/10.14430/arctic71674.

Dansgaard, W. 1964: Stable isotopes in precipitation. *Tellus A: Dynamic Meteorology and Oceanography 16*, 436–468. https://doi.org/10.3402/tellusa.v16i4.8993.

Diekmann, B., Pestryakova, L., Nazarova, L., Subetto, D., Tarasov, P. E., Stauch, G., Thiemann, A., Lehmkuhl, F., Biskaborn, B. K., Kuhn, G., Henning, D. & Müller, S. 2016: Late Quaternary Lake

dynamics in the Verkhoyansk Mountains of eastern Siberia: implications for climate and glaciation history. *Polarforschung 86*, 97–110. https://doi.org/10.2312/polarforschung.86.2.97.

Dodd, J. P. & Sharp, Z. D. 2010: A laser fluorination method for oxygen isotope analysis of biogenic silica and a new oxygen isotope calibration of modern diatoms in freshwater environments. *Geochimica et Cosmochimica Acta 74*, 1381–1390. https://doi.org/10.1016/j.gca.2009.11.023.

Galloway, J. N., Townsend, A. R., Erisman, J. W., Bekunda, M., Cai, Z., Freney, J. R., Martinelli, L. A., Seitzinger, S. P. & Sutton, M. A. 2008: Transformation of the nitrogen cycle: recent trends, questions, and potential solutions. *Science 320*, 889–892. https://doi.org/10.1126/science.1136674.

Gibson, C. E., Anderson, N. J. & Haworth, E. Y. 2003: Aulacoseira subarctica: taxonomy, physiology, ecology and palaeoecology. *European Journal of Phycology 38*, 83–101. https://doi.org/10.1080/0967026031000094102.

Glückler, R., Geng, R., Grimm, L., Baisheva, I., Herzschuh, U., Stoof-Leichsenring, K. R., Kruse, S., Andreev, A., Pestryakova, L. & Dietze, E. 2022: Holocene wildfire and vegetation dynamics in Central Yakutia, Siberia, reconstructed from lake-sediment proxies. *Frontiers in Ecology and Evolution 10*, 962906. https://doi.org/10.3389/fevo.2022.962906.

Glückler, R., Herzschuh, U., Kruse, S., Andreev, A., Vyse, S. A., Winkler, B., Biskaborn, B. K., Pestryakova, L. & Dietze, E. 2021: Wildfire history of the boreal forest of south-western Yakutia (Siberia) over the last two millennia documented by a lake-sediment charcoal record. *Biogeosciences 18*, 4185–4209. https://doi.org/10.5194/bg-18-4185-2021.

Harding, P., Bezrukova, E. V., Kostrova, S. S., Lacey, J. H., Leng, M. J., Meyer, H., Pavlova, L. A., Shchetnikov, A., Shtenberg, M. V., Tarasov, P. E. & Mackay, A. W. 2020: Hydrological (in)stability in Southern Siberia during the Younger Dryas and early Holocene. *Global and Planetary Change 195*, 103333. https://doi.org/10.1016/j.gloplacha.2020.103333.

Herzschuh, U., Böhmer, T., Chevalier, M., Hébert, R., Dallmeyer, A., Li, C., Cao, X., Peyron, O., Nazarova, L., Novenko, E. Y., Park, J., Rudaya, N. A., Schlütz, F., Shumilovskikh, L. S., Tarasov, P. E., Wang, Y., Wen, R., Xu, Q. & Zheng, Z. 2023: Regional pollen-based Holocene temperature and precipitation patterns depart from the Northern Hemisphere mean trends. *Climate of the Past 19*, 1481–1506. https://doi.org/10.5194/cp-19-1481-2023.

Holtgrieve, G. W., Schindler, D. E., Hobbs, W. O., Leavitt, P. R., Ward, E. J., Bunting, L., Chen, G., Finney, B. P., Gregory-Eaves, I., Holmgren, S., Lisac, M. J., Lisi, P. J., Nydick, K., Rogers, L. A., Saros, J. E., Selbie, D. T., Shapley, M. D., Walsh, P. B. & Wolfe, A. P. 2011: A coherent signature of anthropogenic nitrogen deposition to remote watersheds of the Northern Hemisphere. *Science 334*, 1545–1548. https://doi.org/10.1126/science.1212267.

Huang, S., Zhang, K., Lin, Q., Liu, J. & Shen, J. 2022: Abrupt ecological shifts of lakes during the Anthropocene. *Earth-Science Reviews 227*, 103981. https://doi.org/10.1016/j.earscirev.2022.103981.

Hughes-Allen, L., Bouchard, F., Hatté, C., Meyer, H., Pestryakova, L. A., Diekmann, B., Subetto, D. A. & Biskaborn, B. K. 2021: 14,000-year carbon accumulation dynamics in a Siberian Lake reveal catchment and Lake productivity changes. *Frontiers in Earth Science 9*, 710257. https://doi.org/10.3389/feart.2021.710257.

IAEA/WMO 2015: Global network for isotopes in precipitation. The GNIP database. Available at: https://nucleus.iaea.org/wiser (accessed 20.09.2024).

Isaev, A. P., Protopopov, A. V., Protopopova, V. V., Egorova, A. A., Timofeyev, P. A., Nikolaev, A. N., Shurduk, I. F., Lytkina, L. P., Ermakov, N. B., Nikitina, N. V., Efimova, A. P., Zakharova, V. I., Cherosov, M. M., Nikolin, E. G., Sosina, N. K., Troeva, E. I., Gogoleva, P. A., Kuznetsova, L. V., Pestryakov, B. N., Mironova, S. I. & Sleptsova, N. P. 2010: Vegetation of Yakutia: elements of ecology and plant sociology. *In* Troeva, E. I., Isaev, A. P., Cherosov, M. M. & Karpov, N. S. (eds.): *The Far North: Plant Biodiversity and Ecology of Yakutia*, 143–260. Springer Netherlands, Dordrecht.

Kalmychkov, G., Kuz'min, M., Pokrovskii, B. & Kostrova, S. 2007: Oxygen isotopic composition in diatom algae frustules from Lake Baikal sediments: annual mean temperature variations during the last 40 Ka. *Doklady Earth Sciences 413*, 206–209. https://doi.org/10.1134/S1028334X07020158.

Kaufman, D. 2004: Holocene thermal maximum in the western Arctic (0–180°W). *Quaternary Science Reviews 23*, 529–560. https://doi.org/10.1016/j.quascirev.2003.09.007.

Kaufman, D., McKay, N., Routson, C., Erb, M., Datwyler, C., Sommer, P. S., Heiri, O. & Davis, B. 2020: Holocene global mean surface temperature, a multi-method reconstruction approach. *Scientific Data 7*, 201. https://doi.org/10.1038/s41597-020-0530-7.

Kaufman, D. and 95 others 2020: A global database of Holocene paleotemperature records. *Scientific Data 7*, 115. https://doi.org/10.1038/s41597-020-0445-3.

Keeling, C. D. 1979: The Suess effect: 13Carbon-14Carbon interrelations. *Environment International 2*, 229–300. https://doi.org/10.1016/0160-4120(79)90005-9.

Kirillina, K., Shvetsov, E. G., Protopopova, V. V., Thiesmeyer, L. & Yan, W. 2020: Consideration of anthropogenic factors in boreal forest fire regime changes during rapid socio-economic development: case study of forestry districts with increasing burnt area in the Sakha Republic, Russia. *Environmental Research Letters 15*, 35009. https://doi.org/10.1088/1748-9326/ab6c6e.

Kostrova, S. S., Biskaborn, B. K., Pestryakova, L. A., Fernandoy, F., Lenz, M. M. & Meyer, H. 2021: Climate and environmental changes of the Lateglacial transition and Holocene in northeastern Siberia: evidence from diatom oxygen isotopes and assemblage composition at Lake Emanda. *Quaternary Science Reviews 259*, 106905. https://doi.org/10.1016/j.quascirev.2021.106905.

Kostrova, S. S., Meyer, H., Bailey, H. L., Ludikova, A. V., Gromig, R., Kuhn, G., Shibaev, Y. A., Kozachek, A. V., Ekaykin, A. A. & Chapligin, B. 2019: Holocene hydrological variability of Lake Ladoga, northwest Russia, as inferred from diatom oxygen isotopes. *Boreas 48*, 361–376. https://doi.org/10.1111/bor.12385.

Kostrova, S. S., Meyer, H., Chapligin, B., Bezrukova, E. V., Tarasov, P. E. & Kuz'min, M. I. 2013a: Reconstruction of the Holocene climate of Transbaikalia: evidence from the oxygen isotope analysis of fossil diatoms from Kotokel Lake. *Doklady Earth Sciences 451*, 732–736. https://doi.org/10.1134/S1028334x13070039.

Kostrova, S. S., Meyer, H., Chapligin, B., Kossler, A., Bezrukova, E. V. & Tarasov, P. E. 2013b: Holocene oxygen isotope record of diatoms from Lake Kotokel (southern Siberia, Russia) and its palaeoclimatic implications. *Quaternary International 290*, 21–34. https://doi.org/10.1016/j.quaint.2012.05.011.

Kostrova, S. S., Meyer, H., Tarasov, P. E., Bezrukova, E. V., Chapligin, B., Kossler, A., Pavlova, L. A. & Kuzmin, M. I. 2016: Oxygen isotope composition of diatoms from sediments of Lake Kotokel (Buryatia). *Russian Geology and Geophysics 57*, 1239–1247. https://doi.org/10.1016/j.rgg.2016.08.009.

Kruse, S., Bolshiyanov, D., Grigoriev, M. N., Morgenstern, A., Pestryakova, L., Tsibizov, L. & Udke, A. 2019: Russian-German cooperation: expeditions to Siberia in 2018. *In Berichte Zur Polar- Und Meeresforschung = Reports on Polar and Marine Research*. 263 pp. Alfred Wegener Institute for Polar and Marine Research, Bremerhaven. https://doi.org/10.2312/BzPM_0734_2019.

Kurita, N., Yoshida, N., Inoue, G. & Chayanova, E. A. 2004: Modern isotope climatology of Russia: a first assessment. *Journal of Geophysical Research: Atmospheres 109*, D03102. https://doi.org/10.1029/2003jd003404.

Laskar, J., Robutel, P., Joutel, F., Gastineau, M., Correia, A. C. M. & Levrard, B. 2004: A long-term numerical solution for the insolation quantities of the Earth. *Astronomy & Astrophysics 428*, 261–285. https://doi.org/10.1051/0004-6361:20041335.

Leclerc, A. J. & Labeyrie, L. 1987: Temperature dependence of the oxygen isotopic fractionation between diatom silica and water. *Earth and Planetary Science Letters 84*, 69–74. https://doi.org/10.1016/0012-821X(87)90177-4.

Leng, M. J. & Barker, P. A. 2006: A review of the oxygen isotope composition of lacustrine diatom silica for palaeoclimate reconstruction. *Earth-Science Reviews 75*, 5–27. https://doi.org/10.1016/j.earscirev.2005.10.001.

MacDonald, G. M., Kremenetski, K. V. & Beilman, D. W. 2008: Climate change and the northern Russian treeline zone. *Philosophical*

Transactions of the Royal Society, B: Biological Sciences 363, 2285–2299. https://doi.org/10.1098/rstb.2007.2200.

Mackay, A. W., Swann, G. E. A., Brewer, T. S., Leng, M. J., Morley, D. W., Piotrowska, N., Rioual, P. & White, D. 2011: A reassessment of Late Glacial – Holocene diatom oxygen isotope record from Lake Baikal using a geochemical mass-balance approach. *Journal of Quaternary Science 26*, 627–634. https://doi.org/10.1002/jqs.1484.

McLauchlan, K. K., Williams, J. J., Craine, J. M. & Jeffers, E. S. 2013: Changes in global nitrogen cycling during the Holocene epoch. *Nature 495*, 352–355. https://doi.org/10.1038/nature11916.

Meister, P., Alexandre, A., Bailey, H., Barker, P., Biskaborn, B. K., Broadman, E., Cartier, R., Chapligin, B., Couapel, M., Dean, J. R., Diekmann, B., Harding, P., Henderson, A. C. G., Hernandez, A., Herzschuh, U., Kostrova, S. S., Lacey, J., Leng, M. J., Lücke, A., Mackay, A. W., Magyari, E. K., Narancic, B., Porchier, C., Rosqvist, G., Shemesh, A., Sonzogni, C., Swann, G. E. A., Sylvestre, F. & Meyer, H. 2024: A global compilation of diatom silica oxygen isotope records from lake sediment – trends and implications for climate reconstruction. *Climate of the Past 20*, 363–392. https://doi.org/10.5194/cp-20-363-2024.

Messager, M. L., Lehner, B., Grill, G., Nedeva, I. & Schmitt, O. 2016: Estimating the volume and age of water stored in global lakes using a geo-statistical approach. *Nature Communications 7*, 13603. https://doi.org/10.1038/ncomms13603.

Meyer, H., Chapligin, B., Hoff, U., Nazarova, L. & Diekmann, B. 2015a: Oxygen isotope composition of diatoms as Late Holocene climate proxy at Two-Yurts Lake, Central Kamchatka, Russia. *Global and Planetary Change 134*, 118–128. https://doi.org/10.1016/j.gloplacha.2014.04.008.

Meyer, H., Kostrova, S. S., Meister, P., Lenz, M. M., Kuhn, G., Nazarova, L., Syrykh, L. S. & Dvornikov, Y. 2022: Lacustrine diatom oxygen isotopes as palaeo precipitation proxy – Holocene environmental and snowmelt variations recorded at Lake Bolshoye Shchuchye, polar Urals, Russia. *Quaternary Science Reviews 290*, 107620. https://doi.org/10.1016/j.quascirev.2022.107620.

Meyer, H., Opel, T., Laepple, T., Dereviagin, A. Y., Hoffmann, K. & Werner, M. 2015b: Long-term winter warming trend in the Siberian Arctic during the mid- to late Holocene. *Nature Geoscience 8*, 122–125. https://doi.org/10.1038/ngeo2349.

Meyers, P. A. 2009: Organic geochemical proxies. *In* Gornitz, V. (ed.): *Encyclopedia of Paleoclimatology and Ancient Environments. Encyclopedia of Earth Sciences Series*, 659–663. Springer, Dordrecht.

Meyers, P. A. & Teranes, J. L. 2001: Sediment organic matter. *In* Last, W. M. & Smol, J. P. (eds.): *Tracking Environmental Change Using Lake Sediments. Volume 2: Physical and Geochemical Methods*, 239–269. Kluwer Academic Publishers, Dordrecht.

Miesner, T., Herzschuh, U., Pestryakova, L. A., Wieczorek, M., Zakharov, E. S., Kolmogorov, A. I., Davydova, P. V. & Kruse, S. 2022: Forest structure and individual tree inventories of northeastern Siberia along climatic gradients. *Earth System Science Data 14*, 5695–5716. https://doi.org/10.5194/essd-14-5695-2022.

Morley, D. W., Leng, M. J., Mackay, A. W., Sloane, H. J., Rioual, P. & Battarbee, R. W. 2004: Cleaning of lake sediment samples for diatom oxygen isotope analysis. *Journal of Paleolimnology 31*, 391–401. https://doi.org/10.1023/B:JOPL.0000021854.70714.6b.

Moschen, R., Lücke, A. & Schleser, G. H. 2005: Sensitivity of biogenic silica oxygen isotopes to changes in surface water temperature and palaeoclimatology. *Geophysical Research Letters 32*, L07708. https://doi.org/10.1029/2004gl022167.

Müller, S., Tarasov, P. E., Andreev, A. A., Tütken, T., Gartz, S. & Diekmann, B. 2010: Late Quaternary vegetation and environments in the Verkhoyansk Mountains region (NE Asia) reconstructed from a 50-kyr fossil pollen record from Lake Billyakh. *Quaternary Science Reviews 29*, 2071–2086. https://doi.org/10.1016/j.quascirev.2010.04.024.

Nazarova, L., Lüpfert, H., Subetto, D., Pestryakova, L. & Diekmann, B. 2013: Holocene climate conditions in central Yakutia (Eastern Siberia) inferred from sediment composition and fossil chironomids of Lake Temje. *Quaternary International 290-291*, 264–274. https://doi.org/10.1016/j.quaint.2012.11.006.

Obu, J., Westermann, S., Bartsch, A., Berdnikov, N., Christiansen, H. H., Dashtseren, A., Delaloye, R., Elberling, B., Etzelmüller, B., Kholodov, A., Khomutov, A., Kääb, A., Leibman, M. O., Lewkowicz, A. G., Panda, S. K., Romanovsky, V., Way, R. G., Westergaard-Nielsen, A., Wu, T., Yamkhin, J. & Zou, D. 2019: Northern Hemisphere permafrost map based on TTOP modelling for 2000–2016 at 1 km^2 scale. *Earth-Science Reviews 193*, 299–316. https://doi.org/10.1016/j.earscirev.2019.04.023.

Pelánková, B., Kunes, P., Chytry, M., Jankovská, V., Ermakov, N. & Svobodová-Svitavská, H. 2008: The relationships of modern pollen spectra to vegetation and climate along a steppe-forest-tundra transition in southern Siberia, explored by decision trees. *Holocene 18*, 1259–1271. https://doi.org/10.1177/0959683608096600.

Pestryakova, L. A., Herzschuh, U., Gorodnichev, R. & Wetterich, S. 2018: The sensitivity of diatom taxa from Yakutian lakes (northeastern Siberia) to electrical conductivity and other environmental variables. *Polar Research 37*, 1485625. https://doi.org/10.1080/17518369.2018.1485625.

Pestryakova, L. A., Herzschuh, U., Wetterich, S. & Ulrich, M. 2012: Present-day variability and Holocene dynamics of permafrost-affected lakes in central Yakutia (Eastern Siberia) inferred from diatom records. *Quaternary Science Reviews 51*, 56–70. https://doi.org/10.1016/j.quascirev.2012.06.020.

Rantanen, M., Karpechko, A. Y., Lipponen, A., Nordling, K., Hyvärinen, O., Ruosteenoja, K., Vihma, T. & Laaksonen, A. 2022: The Arctic has warmed nearly four times faster than the globe since 1979. *Communications Earth & Environment 3*, 168. https://doi.org/10.1038/s43247-022-00498-3.

Renssen, H., Seppä, H., Heiri, O., Roche, D. M., Goosse, H. & Fichefet, T. 2009: The spatial and temporal complexity of the Holocene thermal maximum. *Nature Geoscience 2*, 411–414. https://doi.org/10.1038/ngeo513.

Roberts, S. L., Swann, G. E. A., McGowan, S., Panizzo, V. N., Vologina, E. G., Sturm, M. & Mackay, A. W. 2018: Diatom evidence of 20th century ecosystem change in Lake Baikal, Siberia. *PLoS One 13*, e0208765. https://doi.org/10.1371/journal.pone.0208765.

Roland, T. P., Daley, T. J., Caseldine, C. J., Charman, D. J., Turney, C. S. M., Amesbury, M. J., Thompson, G. J. & Woodley, E. J. 2015: The 5.2 ka climate event: evidence from stable isotope and multi-proxy palaeoecological peatland records in Ireland. *Quaternary Science Reviews 124*, 209–223. https://doi.org/10.1016/j.quascirev.2015.07.026.

Scholten, R. C., Coumou, D., Luo, F. & Veraverbeke, S. 2022: Early snowmelt and polar jet dynamics co-influence recent extreme Siberian fire seasons. *Science 378*, 1005–1009. https://doi.org/10.1126/science.abn4419.

Shestakova, A. A., Fedorov, A. N., Torgovkin, Y. I., Konstantinov, P. Y., Vasyliev, N. F., Kalinicheva, S. V., Samsonova, V. V., Hiyama, T., Iijima, Y., Park, H., Iwahana, G. & Gorokhov, A. N. 2021: Mapping the Main characteristics of permafrost on the basis of a permafrost-landscape map of Yakutia using GIS. *Land 10*, 462. https://doi.org/10.3390/land10050462.

Solomina, O. N., Bradley, R. S., Hodgson, D. A., Ivy-Ochs, S., Jomelli, V., Mackintosh, A. N., Nesje, A., Owen, L. A., Wanner, H., Wiles, G. C. & Young, N. E. 2015: Holocene glacier fluctuations. *Quaternary Science Reviews 111*, 9–34. https://doi.org/10.1016/j.quascirev.2014.11.018.

Stevenson, M. A., McGowan, S., Pearson, E. J., Swann, G. E. A., Leng, M. J., Jones, V. J., Bailey, J. J., Huang, X. & Whiteford, E. 2021: Anthropocene climate warming enhances autochthonous carbon cycling in an upland Arctic lake, Disko Island, West Greenland. *Biogeosciences 18*, 2465–2485. https://doi.org/10.5194/bg-18-2465-2021.

Stieg, A., Biskaborn, B. K., Herzschuh, U., Marent, A., Strauss, J., Wilhelms–Dick, D., Pestryakova, L. A. & Meyer, H. 2024a: Diatom shifts and limnological changes in a Siberian boreal lake: impacts of climate warming and anthropogenic pollution. *EGUsphere, Copernicus Publications 2024*, 1–39. https://doi.org/10.5194/egusphere-2024-2470.

Stieg, A., Biskaborn, B. K., Herzschuh, U., Strauss, J., Pestryakova, L. & Meyer, H. 2024b: Hydroclimatic anomalies detected by a sub-decadal diatom oxygen isotope record of the last 220 years from

Lake Khamra, Siberia. *Climate of the Past 20*, 909–933. https://doi.org/10.5194/cp-20-909-2024.

Subetto, D. A., Nazarova, L. B., Pestryakova, L. A., Syrykh, L. S., Andronikov, A. V., Biskaborn, B., Diekmann, B., Kuznetsov, D. D., Sapelko, T. V. & Grekov, I. M. 2017: Paleolimnological studies in Russian northern Eurasia: a review. *Contemporary Problems of Ecology 10*, 327–335. https://doi.org/10.1134/s1995425517040102.

Swann, G. E. A. & Leng, M. J. 2009: A review of diatom $\delta^{18}O$ in palaeoceanography. *Quaternary Science Reviews 28*, 384–398. https://doi.org/10.1016/j.quascirev.2008.11.002.

Swann, G. E. A., Leng, M. J., Juschus, O., Melles, M., Brigham-Grette, J. & Sloane, H. J. 2010: A combined oxygen and silicon diatom isotope record of Late Quaternary change in Lake El'gygytgyn, North East Siberia. *Quaternary Science Reviews 29*, 774–786. https://doi.org/10.1016/j.quascirev.2009.11.024.

Swann, G. E. A., Mackay, A. W., Vologina, E., Jones, M. D., Panizzo, V. N., Leng, M. J., Sloane, H. J., Snelling, A. M. & Sturm, M. 2018: Lake Baikal isotope records of Holocene central Asian precipitation. *Quaternary Science Reviews 189*, 210–222. https://doi.org/10.1016/j.quascirev.2018.04.013.

Tarasov, P., Bezrukova, E., Karabanov, E., Nakagawa, T., Wagner, M., Kulagina, N., Letunova, P., Abzaeva, A., Granoszewski, W. & Riedel, F. 2007: Vegetation and climate dynamics during the Holocene and Eemian interglacials derived from Lake Baikal pollen records. *Palaeogeography, Palaeoclimatology, Palaeoecology 252*, 440–457. https://doi.org/10.1016/j.palaeo.2007.05.002.

Tarasov, P. E., Müller, S., Zech, M., Andreeva, D., Diekmann, B. & Leipe, C. 2013: Last glacial vegetation reconstructions in the extreme-continental eastern Asia: potentials of pollen and n-alkane biomarker analyses. *Quaternary International 290-291*, 253–263. https://doi.org/10.1016/j.quaint.2012.04.007.

Tchebakova, N. M., Parfenova, E. & Soja, A. J. 2009: The effects of climate, permafrost and fire on vegetation change in Siberia in a changing climate. *Environmental Research Letters 4*, 045013. https://doi.org/10.1088/1748-9326/4/4/045013.

Walker, M., Johnsen, S., Rasmussen, S. O., Popp, T., Steffensen, J. P., Gibbard, P., Hoek, W., Lowe, J., Andrews, J., Björck, S., Cwynar, L. C., Hughen, K., Kershaw, P., Kromer, B., Litt, T., Lowe, D. J., Nakagawa, T., Newnham, R. & Schwander, J. 2009: Formal definition and dating of the GSSP (Global Stratotype Section and Point) for the base of the Holocene using the Greenland NGRIP ice core, and selected auxiliary records. *Journal of Quaternary Science 24*, 3–17. https://doi.org/10.1002/jqs.1227.

Wang, L., Mackay, A. W., Leng, M. J., Rioual, P., Panizzo, V. N., Lu, H., Gu, Z., Chu, G., Han, J. & Kendrick, C. P. 2013: Influence of the ratio of planktonic to benthic diatoms on lacustrine organic matter $\delta^{13}C$ from Erlongwan maar lake, northeast China. *Organic Geochemistry 54*, 62–68. https://doi.org/10.1016/j.orggeochem.2012.09.010.

Wolfe, A. P., Hobbs, W. O., Birks, H. H., Briner, J. P., Holmgren, S. U., Ingólfsson, Ó., Kaushal, S. S., Miller, G. H., Pagani, M., Saros, J. E. & Vinebrooke, R. D. 2013: Stratigraphic expressions of the Holocene–Anthropocene transition revealed in sediments from remote lakes. *Earth-Science Reviews 116*, 17–34. https://doi.org/10.1016/j.earscirev.2012.11.001.

Woolway, R. I., Kraemer, B. M., Lenters, J. D., Merchant, C. J., O'Reilly, C. M. & Sharma, S. 2020: Global lake responses to climate change. *Nature Reviews Earth and Environment 1*, 388–403. https://doi.org/10.1038/s43017-020-0067-5.